UNIVERSITÀ DEGLI STUDI DI PADOVA

Dipartimento di Fisica e Astronomia "Galileo Galilei"

Master Degree in Physics

Final Dissertation

Drop motion optically induced on photorefractive surfaces

Thesis supervisor

Prof. Matteo Pierno

Thesis co-supervisor

Prof. Giampaolo Mistura

Dr. Davide Ferraro

Candidate

Sebastian Cremaschini

Academic Year 2020/2021

Contents

Introduction

Microfluidics is aimed to manipulate and control the motion of droplets with volumes ranging from 10^{-9} to 10^{-6} L for applications in a variety of fields such as medicine, biology or industry [1]. Thanks to microfabrication techniques advancements nowadays it is possible to realize microfliuidic devices, where droplets can be easily generated, driven in their motion and analyzed. This kind of devices can be realized in a closed configuration, where droplets are confined in properly shaped microchannels or an open configuration, where droplets can be put in motion over a specific substrate by controlling its wettability up to the micron scale [2].

In open microfluidics the motion of droplets should occur over a solid surface, but due to the defects of the surface itself (the roughness in particular) droplets can experience the phenomenon of pinning over surface defects and as a consequence controlling the movement of the fluid becomes very hard. In the natural world there are some examples of plants, whose leaves are characterized by self-cleaning and slippery properties such as in the cases of Lotus [4] or Nepenthes pitcher plants [5]. For this reason specific surfaces, that mimic the behaviours of some plants belonging to the natural world, have been developed: called **Liquid-Infused Surfaces (LIS)** these are porous surfaces impregnated with a specific lubrificant oil (see in Fig. 1). The LIS is a liquid surface so it's intrinsically smooth down to the atomic scale and it's also a defect free surface; as a consequence it's main advantage is to reduce the friction force, that a moving body over that surface would be affected. A water droplet, which is immiscible with the oil forming the LIS, would be easily put in motion and then manipulate over this kind of specific surface [6].

Figure 1: Example of drop motion over a LIS [3].

The most commonly technique to tune the wetting properties of a surface, is electrowetting: it consists in applying a voltage difference between the substrate and the droplet, so that apparently the wettability of the surface itself is modified and droplets can be put in motion and be forced to follow the pattern of charges created thanks to the electrodes [7]. In order to avoid the electrolysis of droplets at the metallic surface and that the water droplet could screen the charges accumulated in the substrate, a thin dielectric film between the liquid and the solid surface can be added. This trick is at the basis of the technique called electrowetting-on a dielectric (EWOD). However these methods has two main drawbacks: first fixed metallic electrode are used so the system isn't characterized by a high degree of reconfigurability and then expensive facilities are required for the production of this kind of devices (such as photolitographic techniques for the patterning of electrodes inside the sample or the realization of the proper electrical circuit in order to apply the desired voltage difference to the system).

To overcome these limitations, a novel technique has been developed and called **optowetting (OW)**: it consists in generating virtual reconfigurable electrodes by simply illuminating a specific

material with the chosen light pattern. A convenient material for the realization of optowetting is Lithium Niobate ($LiNbO_3$): these material is characterized by interesting non-linear optical (birefringence and anisotropy) and electrical (piezoelectric and pyroelectric effect) properties and the most important one for the optowetting technique is called photovoltaic effect. When the Lithium niobate is illuminated thanks to visible coherent light (in general), free electric charges start to move from the valence band towards the conduction band of the crystal and as a consequence an electric current and an electric field are created inside the material [8]. The motion of charges (electrons in particular) occurs in one preferred direction, parallel to the crystallographic axis (the $\hat{c}$-axis), since $LiNbO_3$ is a non-centrosimmetryc material. In Fig. 2 there is a comparison betweeen an electrowetting scheme (a) and an optowetting one (b).
The photovoltaic effect can be enhanced by doping the material using transition metals and the most common dopant material is Iron: the addition of Fe ions allows to increase the electric field up to 10^6 V m^{-1} and knowing the reduction degree of the Iron dopant it's possible to trying to control the typical time constant of the photovoltaic effect. The electric fields generated due to this characteristic effect of Lithium Niobate can be exploited to control the motion of dielectric particles or water droplets using the electrophoretic or dielectrophoretic effects in order to manipulated charged or neutral objects respectively.
Previous works [9] display that the photovoltaic properties of Lithium Niobate could be affected by the environmental conditions of the laboratory, in which the measurements are performed; in particular it's possible to focus the attention over humidity. No research group in the world has realized a systematic study of the role of humidity on $LiNbO_3$ discharge, when a specific illumination pattern is switched off and as a consequence in literature there are no scientific articles, describing this effect properly.

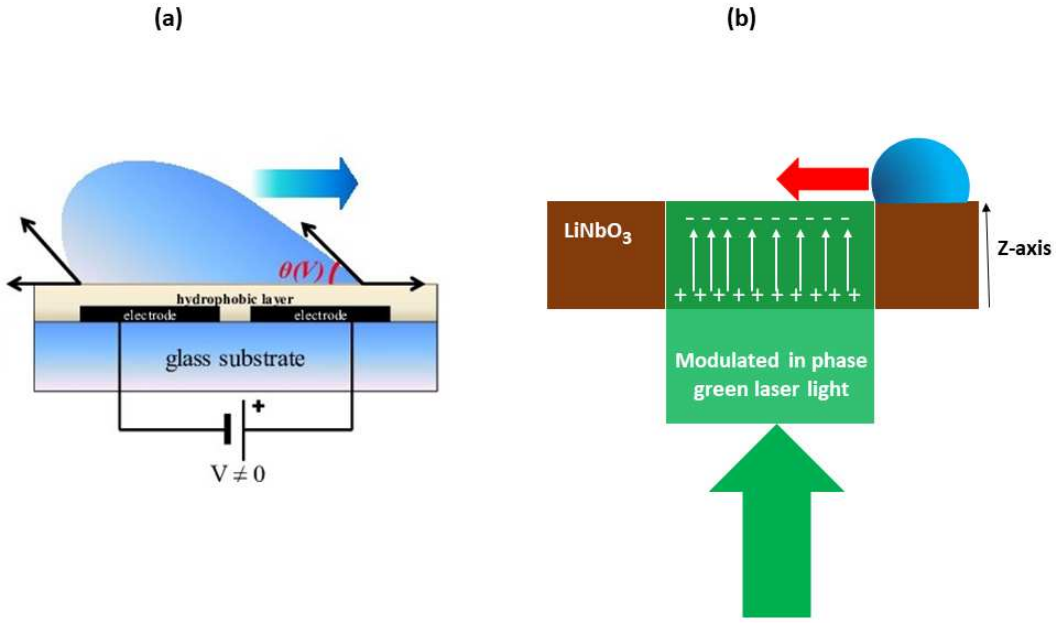

Figure 2: (a) electrowetting example [10]; (b) optowetting example

The main goal of this thesis work is to exploit the optowetting method in order to control the motion of water droplets over a horizontal and not tilted plane; due to this last experimental condition the motion control becomes an active process since gravity doesn't play an important role in moving droplets. Lithium Niobate is the material chosen as part of the experimental

sample and the electric field generated due to photovoltaic effect is exploited to control the motion of neutral water droplets (thanks to the dielectrophoretic effect). Since $LiNbO_3$ is a solid surface, in order to avoid the pinning of droplets over surface defects, a specific coating is realized over the surface of the material in order to create a liquid-infused surface. The illumination of the sample is obtained thanks to a green diode-pumped laser and the desired illumination pattern is projected over the sample using a spatial light modulator (SLM): this device receives laser light in input, it modulates this light in phase and allows to create the desired illumination pattern of the sample.

The experimental measurements are divided in two main parts: (i) the role of humidity over the discharge of $LiNbO_3$, when the illumination pattern is switched off, is investigated by studying the behaviour of pendant droplets generated over the previously illuminated region of the sample and then falling due to dielectrophoretic effect. After that the humidity condition for which the effect of humidity over Lithium Niobate discharge is less relevant is chosen and the next measurements are performed in this specifically controlled environmental condition. (ii) The second part of the measurements aims to put in motion water droplets and then realize specific processes: first the attraction of droplets towards an illumination pattern is studied; then water droplets are put in motion and forced to follow a specific path (linear or curved). After that the merging process of two or three droplets is realized. Finally the splitting of a droplet and the motion of a droplet over a non-homogeneously illuminated pattern are studied.

Outline of the thesis

This thesis project is organized as follows:

- **Chapter 1**: the main theoretical concepts of wetting are described; then a brief description of the electrowetting technique is given and the concept of Liquid-Infused Surface (LIS) is introduced.
- **Chapter 2**: the main properties and effects of Lithium Niobate are described; in particular a detailed description of the photovoltaic effect is given.
- **Chapter 3**: the experimental set-up is described in details, focusing the attention over the $LiNbO_3$ sample, the realization of the LIS and how a SLM works.
- **Chapter 4**: the experimental data are presented and discussed.

This thesis activity took place during the second semester of the academic year 2020-2021 from March to September 2021 at the Laboratorio di Fisica delle Superfici ed Interfacce (LaFSI) and was a collaboration of this group and the $LiNbO_3$ group inside the Department of Physics and Astronomy at the University of Padua.

Chapter 1

Wetting

1.1 Interfaces and surface tension

An interface is a surface that separates 2 different media like for example a water droplet and air or a water droplet and a solid surface.
The surface tension emerges from the discontinuity of density between 2 immiscibile fluids and this discontinuity is related to the unbalance of the intermolecular forces between molecules [11]. The molecules can be found in the bulk state, where they are surrounded by other molecules or at the interface, where the molecules can interact with only half of the other molecules below (example in Fig. 1.1).

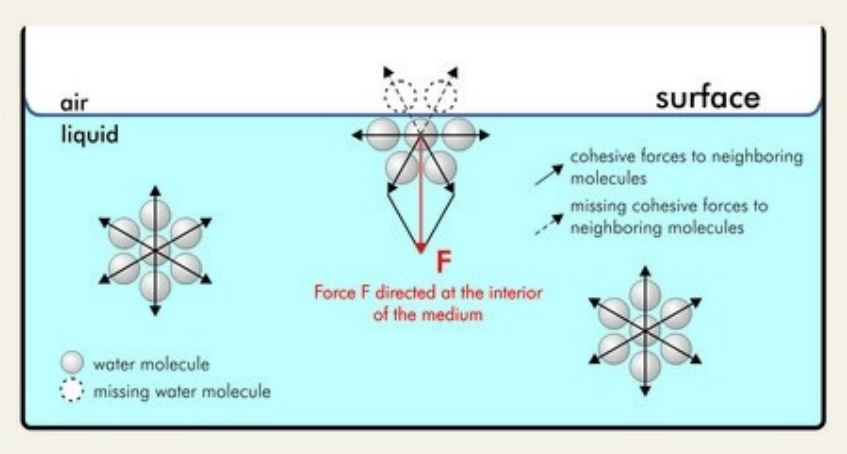

Figure 1.1: Bulk molecule vs molecule at the interface [11].

The molecules in the bulk state are characterized by a total energy U; instead the molecules at the interface has a total energy equal to $U/2$; so a molecule loses $1/2$ of his total energy moving from the bulk to the interface. As a consequence the surface tension γ is given by $\gamma = U/2a^2$, where a is the characteristic molecular size and the surface tension measures directly the energy fall per unit area for a moving droplet from bulk to the interface.
Moreover another reasoning can be performed in order to understand the role of the surface tension: if the surface of an interface needs to be increased of a quantity δA, the external work (δW) to apply is directly proportional to the quantity δA and the constant of proportionality is given the surface tension γ itself. The following relation holds:

$$\delta W = \gamma \delta A$$

From a thermodynamic point of view the surface tension can be defined in terms of the free energy with the following relation by fixing temperature T, volume V and number of molecules n:

$$\gamma = \left(\frac{\partial F}{\partial A}\right)_{T,V,n}$$

The surface tension can be directly linked to the difference in pressure Δp across the the curved surface between two different liquids using the Young-Laplace's law [11]:

$$\Delta p = \gamma \left(\frac{1}{R_1} + \frac{1}{R_2}\right)$$

where R_1 and R_2 are the 2 radii of curvature of the interface.
The surface tension can be used to define two dimensionless number very important in the field of microfluidics:

- the Bond number Bo is given by the following expression:

$$Bo = \frac{\rho g L^2}{\gamma} = \left(\frac{L}{\lambda_c}\right)^2$$

  where g is the gravity acceleration, ρ is the fluid density, L is the characteristic length of system considered and λ_c is the capillary length, which defines the spatial length below which the effect of gravity can be discarded. The capillary length λ_c is defined in the following way:

$$\lambda_c = \sqrt{\frac{\gamma}{\rho g}}$$

  As a consequence if the Bond number is greater than 1, gravity dominates over surface tension effects; instead in the opposite case gravity effects can be neglected safely.

- In the case of moving droplets, the capillary number Ca is defined as the ratio between viscous forces over capillary forces and its mathematical expression is the following:

$$Ca = \frac{\mu v}{\gamma}$$

  where μ is the dynamic viscosity of the droplet itself. If the capillary number is less than 1 capillary effects dominate over viscous forces.

1.2 Wetting on surfaces

The typical configuration used to describe the wetting on a surface is the one in Fig. 1.2, where there is a water droplet lying on a solid substrate; in this image it is possible to identify 3 different interfaces: liquid-solid, liquid-air and air-solid.
Considering the interaction between solid and liquid, it's possible to distinguish 2 different regimes of wetting, complete or incomplete, and the parameter used to distinguish between them is called Spreading parameter (S), which is defined as the difference in energy when the substrate is dry (E_{dry}) and when it's wet (E_{wet}):

$$S = E_{dry} - E_{wet}$$

or in an alternative way

$$S = \gamma_{SV} - (\gamma_{SL} + \gamma_{LV})$$

where γ_{SV} is the surface tension between solid and air, γ_{SL} is the surface tension between solid and liquid and γ_{LV} is the surface tension between liquid and air. In the case $S>0$ the configuration of total wetting is found, instead in the opposite case the liquid does not wet the substrate completely (partial wetting) and a contact angle θ of the liquid on the solid substrate is formed. This contact angle is obtained considering the mechanical equilibrium among the forces acting on the surface and this leads to Young's equation [12]:

$$\gamma_{LV} cos(\theta) = \gamma_{SV} - \gamma_{SL}$$

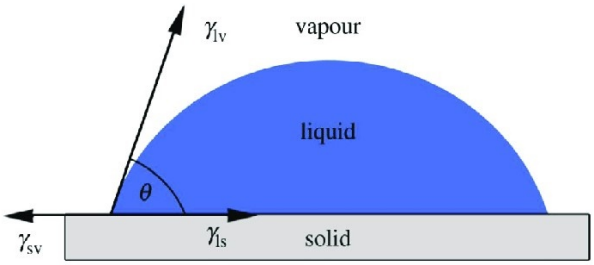

Figure 1.2: three-phase interface with relative contact angle [13].

The contact angle, measured when a water droplet is put on a solid substrate, is the parameter used to describe the wettability over a surface and allows to distinguish between different kinds of surface (Fig. 1.3) [13]:

- complete wetting, when the contact angle is exactly 0°;
- superhydrophilic surface, when the contact angle is lower than 5°;
- hydrophilic surface, when the contact angle is lower than 90°;
- hydrophobic surface, when the contact angle is between 90° and 150°;
- superhydrophobic surface, when the contact angle is greater than 150°.

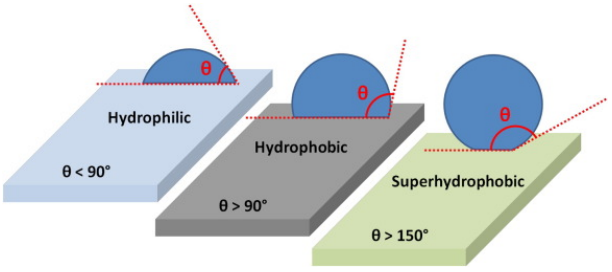

Figure 1.3: Some examples of wetting regimes [14].

The hydrophobyc or hydrophilic nature of a surface depends on the chemistry of the surface itself and as a consequence changing the chemical nature of the surface could lead to the desired wetting condition. In particular a superhydrophobic surface also requires the presence of roughness on the surface at the micro/nano scale.

1.3 Contact angle hysteresis

In an ideal case when a droplet is put on a surface, it should always form the same static contact angle at equilibrium; but in reality each surface is characterized by defects and inhomogeneities and as a consequence the static contact angle at equilibrium could change, assuming values in a certain range. The contact angle hysteresis δ_H is defined in the following way:

$$\delta_H = \theta_A - \theta_R$$

where θ_A is the advancing angle, which is the maximum angle above which the front meniscus stats to advance and θ_R is the receding angle, which is the minimum angle below which the back meniscus starts to recede. The critical sliding angle of a surface α is defined as the minimum tilting angle of the surface itself so that the droplet starts to move [15]. The contact angle hysteresis is deeply related to the movement of a droplet: low hysteresis means that the interaction between the liquid and the solid surface is weak and as a consequence the droplet can easily move; on the contrary in the case of high hysteresis the droplet cannot be put in motion in an easy way because there is a strong interaction between the 2 involved phases related to the roughness and defects of the solid substrate.

1.4 Liquid infused surface (LIS)

In order to favor the motion of a droplet over a surface, it's required to reduce the contact angle hysteresis. In the last years different methods were tried in order to reach the desired goal taking inspiration from the natural world, where some plants are characterized by interesting self-cleaning or hydro-repellent properties [16]. As an example, the lotus leaves present a characteristic roughness over the surface, so that a droplet doesn't interact with a solid surface anymore, but an air cushion forms below the droplet itself and as a consequence the friction is drastically reduced.
In nature there is another plant with interesting properties: the Nepenthes pitcher plant: its peristomes are impregnated with a liquid able to attract insects. If the insect touches the liquid, it remains trapped in and it slides down inside the plant, where it's eaten by the plant itself [5]. The laboratory's replica of surfaces, mimicking the interesting properties of Lotus' or Nepenthes pitcher leaves, leads to the realization of the so called liquid infused surfaces (LIS) or slippery liquid infused porous surfaces (SLIPS) [17], which are specifically structured solid materials impregnated with lyophilic oil. This textured surfaces can be realized in a laboratory with different methods such as using Teflon membranes or exploiting photolithographic techniques in order to realize regular arrays of properly shaped micro/nano-structures [18], [19]. The main advantages of the LIS are that a liquid surface is incompressible, it can self-repair damages and is a defect-free surface. If the lubrificant oil is not added to these microstructured solid surfaces, the droplet could experience the pinning phenomenon over the surface defects; the addition of the lubrificant oil reduces the pinning and the contact angle hysteresis, favoring droplet motion.
A drop over a LIS is a system characterized by four different phases: the structured solid, the lubrificant oil, the droplet itself and the air around the system [20]. In the sequence of images in Fig. 1.4 there some typical examples, that can occur when a droplet is lying over a LIS. The droplet can be in direct contact with solid surface (images c and d), forming a solid-contact line or the lubrificant film can avoid this situation (images a and b). The droplet could be surrounded entirely by the lubrificant oil, forming a cloak (images a and c) or the oil could generate an annular wetting ridge around the droplet itself, giving rise to a liquid contact-line (images b and d).

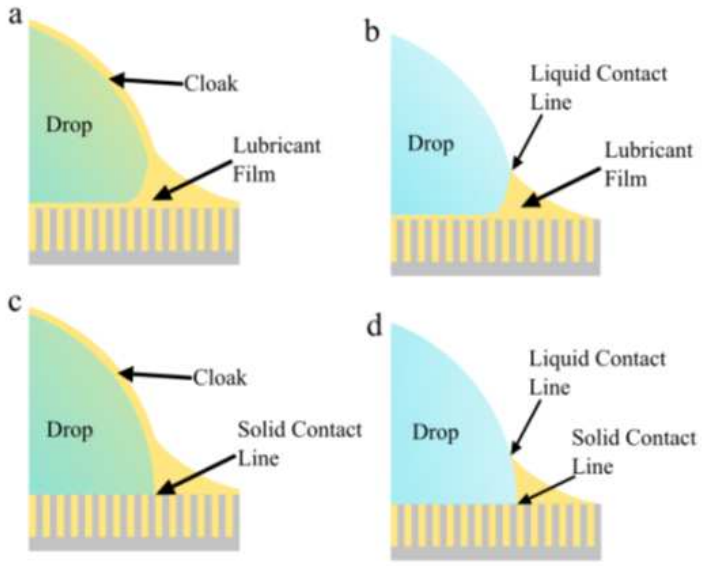

Figure 1.4: Possible wetting configurations over a LIS [17].

In order to have a stable impregnation the contact angle formed between the oil and the impregnated solid surface needs to be lower than a critical angle θ_c, defined by the following relation:

$$\theta_c = cos^{-1}\left(\frac{1-\phi}{r-\phi}\right)$$

where ϕ is the fraction of solid area in contact with the droplet and r is the roughness of the surface itself.
Because of its properties, the LIS can be exploited for different applications such as the realization of anti-icing, anti-fogging or anti-biofouling coatings [21], [22].

1.5 Electrowetting

One of the main goals of open microfluidics is manipulating droplets over a solid substrate, controlling their motion, sorting, merging or splitting for applications in the field of chemistry, biology or medicine. Droplet manipulation can be obtained by controlling the interfacial energy between the liquid droplet and the underlying substrate.
The most used technique used in the last 2 decades in order to manipulate droplets is called electrowetting: historically the first devices were characterized by two metallic electrodes put in contact with the droplet [23]. The application of a voltage difference between the 2 electrodes gives rise to the accumulation of charges in the metallic surface and as a consequence an electric double layer at the solid-liquid interface is formed [7]. But this technique has a problem: in fact the water droplet can "screen" the charges accumulated in the metallic surface, so that the desired phenomenon cannot occur. Furthermore if the voltage difference applied overcomes a certain threshold, the water droplet could experience the phenomenon of electrolysis, making the system really unstable.
In order to solve the problem Berge introduced a thin insulating layer to divide the liquid from the metallic electrode below, giving birth to a new technique called electrowetting-on-dielectric (EWOD) [23]. In this configuration applying an electric field, the voltage drop occurs inside the dielectric layer, preventing the screening effect of the charges due to the water droplet. This kind

of electrostatic interaction causes the reduction of the contact angle formed by the droplet over the substrate, meaning that there is an apparent change in the wettability at the solid-liquid interface (as shown in Fig. 1.5).

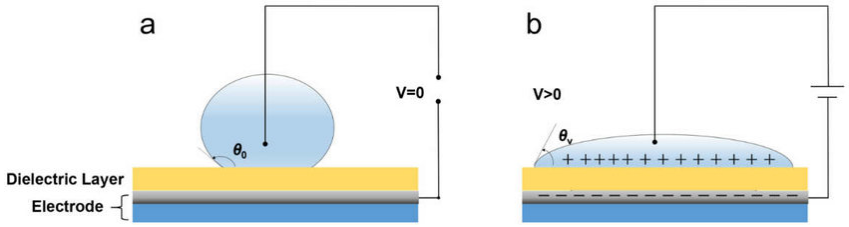

Figure 1.5: Typical example of electrowetting on a dielectric: in figure (a) no voltage applied; in figure (b) a voltage V>0 is applied [24].

For low voltage values, the effective surface tension between the solid and the liquid is given by:

$$\gamma_{SL}^{eff} = \gamma_{SL} - \frac{\epsilon_0 \epsilon_d}{2d} V^2$$

where γ_{SL} is the surface tension in absence of voltage difference, ϵ_d is the dielectric constant of the insulator, d is the thickness of the insulating layer and V is the applied voltage difference. From the previous expression it's possible to derive the Young-Lippman equation for the variation of contact angle:

$$cos(\theta) = cos(\theta_Y) + \frac{\epsilon_0 \epsilon_d}{2d\gamma_{LV}} V^2$$

where γ_{LV} is the surface tension between liquid and vapor.
Beyond a certain threshold, the contact angle value becomes independent on the voltage difference applied (contact angle saturation).
In the standard electrowetting configuration droplet movement is not so easy to obtain since that the process should occur over a solid surface characterized by inhomogenities and defects (roughness in particular). In order to overcome the previous problem anew technique has been developed and called electrowetting on liquid-infused film (EWOLF), in which the dielectric insulating layer (a solid surface) is substituted by a thin insulating liquid surface [25]. By definition a liquid surface is an atomically flat and a defect-free surface; for this reason in principle it should be easier to put in motion a water droplet on a liquid surface with respect to the case of a solid substrate (an example of electrowetting to move a water droplet is shown in Fig. 1.6).

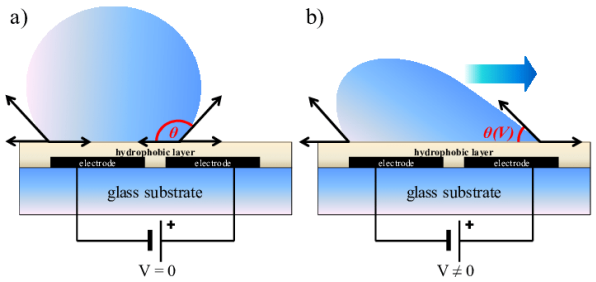

Figure 1.6: Example of elettrowetting to put a water droplet in motion [10].

Chapter 2

Lithium niobate

2.1 Chemical composition

Lithium Niobate ($LiNbO_3$ or LN in the following) is a synthetic material discovered as one of the fundamental compounds of the pseudo-binary system Li_2-Nb_2O_5 at the Bell Labs in 1928. At room temperature Lithium Niobate crystals appears in a solid form and moreover they are colourless, chemically stable and insoluble in water or other organic solvents. Furthermore this material behaves as an insulator at any temperature and it is characterized by an energy gap of about 4 eV.
It's possible to construct a phase diagram for different temperatures by changing the percentages of the 2 oxydes in the system Li_2-Nb_2O_5 (this phase diagram is shown in Fig. 2.1).

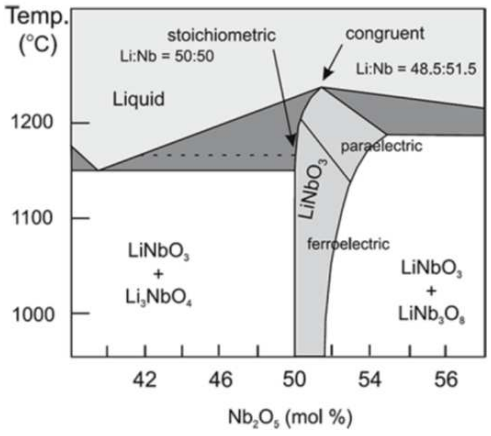

Figure 2.1: Phase diagram of the pseudo-binary system Li_2-Nb_2O_5 [26].

By observing the previous diagram, it's possible to notice that the congruent composition of the crystal (where there is a Lithium deficiency with respect to Niobium) behaves as the maximum of the solid-liquid curve. Instead in the stoichiometric composition, the 2 oxydes Li_2O and Nb_2O_5 are present with the same percentage in the crystal.
The ratio between the concentrations of Li and Nb influences different properties of Lithium Niobate such as phase transition temperature, birefringence, the photovoltaic effect or the absorption in the UV range [26].

2.2 Crystal structure

From the crystallographic point of view Lithium Niobate's structure can be described thanks to 3 different cells: the hexagonal, the rhomboedral or the orthohexagonal one. The most commonly used is the orthohexagonal structure (shown in Fig. 2.2), but in some applications it's more convenient to refer to the other 2 cells.
At room temperature the crystal is characterized by a mirror symmetry around 3 planes, rotated 60° one with respects to the others. It's possible to define 3 mutually orthogonal Cartesian axes related to the orthohexagonal cell:

- $\hat{z}$-axis, commonly defined as the optical axis or $\hat{z}$-axis of the system, around which the $LiNbO_3$ shows its three-fold rotation symmetry;
- $\hat{y}$-axis, belonging to one of the 3 mirror planes;
- $\hat{x}$-axis, perpendicular to the 2 previous axes.

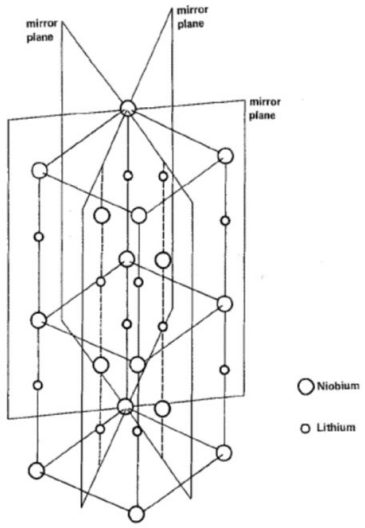

Figure 2.2: Orthohexagonal crystalline structure of Lithium Niobate [8].

The positive directions of $\hat{z}$ and $\hat{y}$ axes point towards the crystal surface, becoming negatively charged under compression ans so both axes are related to piezoelectric properties of LN. Moreover the $\hat{z}$-axis is related to pyroelectricity and its positive direction points towards the plane becoming positively charged when the crystal is cooled down.
The crystalline structure of $LiNbO_3$ is deeply influenced by temperature and in fact 2 different configurations exist:

- for temperature values over the Curie temperature the material is found in the paraelectric phase, in which the Oxygen atoms form equilateral triangular configurations rotated of 180° one with respect to the other, belonging to planar sheets along the $\hat{c}$-axis. Lithium ions are in the middle of the equilateral triangles made of Oxygen atoms; instead Niobium atoms are in the middle of the tridimensional octaedral formed by joining the vertexes of 2 triangles lying on 2 parallel and different planes. In this phase the material does not display a spontaneous polarization (Fig. 2.3 (a)).
- Instead for temperatures over the the value of the Curie temperature, Lithium Niobate appears in the ferroelectric phase, in which Niobium and Lithium ions move a little bit

along the direction of the$\hat{c}$-axis of the crystal with respect of the crystalline structure in the paraelectric phase. The interstices formed between Oxygen planes are occupied one-third by Lithium ions, one-third by Niobium ions and one-third displays a vacancy. In this configuration Lithium Niobate displays a spontaneous polarization dependent on the value of the temperature, that can be reversed by applying high electric fields in the direction opposite to the spontaneous polarization of the crystal (Fig. 2.3 (b)).

Moreover in the congruent composition some Nb ions can occupy Li lattice sites, that are empty because of the lower percentage of Li with respect to the percentage of Nb in the material and these ions are called Nb-antisites and can affect the photovoltaic properties of lithium niobate.

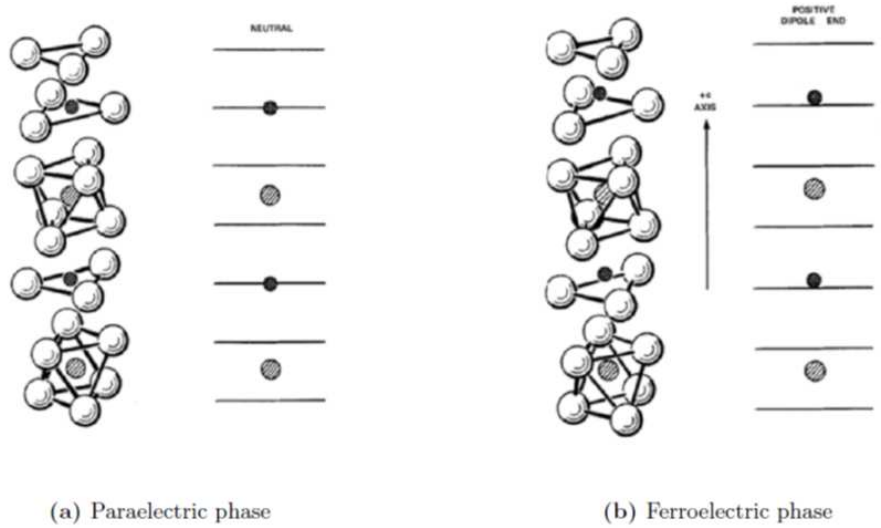

(a) Paraelectric phase (b) Ferroelectric phase

Figure 2.3: 2 different phases of Lithium Niobate. O ions are shown with white big circles, small dark circles represent Li ions and Nb ions are represented with single-cross hatched circles [8].

2.3 Physical properties

In this section the most relevant properties of Lithium Niobate will be described; in particular a detailed description of the photovoltaic effect, (exploited to perform the experimental measurements described in the next sections) will be given.

2.3.1 Birefringence

Lithium Niobate is an anisotropic material, for which the optical response from an external electric field is obtained by considering the electric displacement vector through the dielectric permittivity tensor:

$$\mathbf{D} = \hat{\epsilon}\mathbf{E}$$

where $\mathbf{D}$ is the displacement vector, $\mathbf{E}$ is the electric field vector and $\hat{\epsilon}$ is the dielectric tensor. In the case of Lithium Niobate the dielectric tensor with respect to the principal axes is given

by:

$$\begin{bmatrix} \epsilon_{11} & 0 & 0 \\ 0 & \epsilon_{11} & 0 \\ 0 & 0 & \epsilon_{33} \end{bmatrix}$$

The ordinary refractive index (n_o), referring to the $\hat{x}$ and $\hat{y}$ directions, and the extraordinary refractive index (n_e), related to the $\hat{z}$ direction, are functions only of the 2 coefficients appearing in the dielecric tensor:

$$n_o = \sqrt{\frac{\epsilon_{11}}{\epsilon_0}} \qquad\qquad n_e = \sqrt{\frac{\epsilon_{33}}{\epsilon_0}}$$

where ϵ_0 is the vacuum dielectric permeability. Lithium Niobate is a birefringent material since the 2 refractive indexes are different one from each other; moreover the law of dispersion is deeply affected by temperature and the concentration of Li atoms in the material [27].

2.3.2 Electro-optic effect

The electro-optic effect is a second-order optical phenomenon and describes the change of the refractive index value of a material, when it's exposed to a high external electric field. This variation can be mathematically described by a power series with respect to the electric field E:

$$\Delta(\frac{1}{n^2})_{ij} = \sum_k r_{ijk}E_k + \sum_{k,l} s_{ijkl}E_kE_l$$

where the tensors r_{ijk} and s_{ijkl} describe respectively the linear (Pockels) and quadratic (Kerr) contributions to the electro-optic effect.
In the case of electric fields, which are not very intense, this effect is linear and also depends on the polarization of incident light. In particular if the light is polarized along the optical axis and propagates along $\hat{x}$ or $\hat{y}$ axes, the variations of the refractive indexes are described by:

$$\Delta n_o = -\frac{n_o^3 r_{13} E_z}{2} \qquad\qquad \Delta n_e = -\frac{n_e^3 r_{33} E_z}{2}$$

and in the case of light propagating along $\hat{z}$ direction and polarized along $\hat{x}$ or $\hat{y}$ directions the variations of the refractive indices are given by:

$$\Delta n_o = -\frac{n_o^3 r_{22} E_x}{2} \qquad\qquad \Delta n_e = 0$$

2.3.3 Piezolecetric effect

Lithium Niobate displays the piezoelectric effect: when a mechanical stress is applied to the material, a polarization is induced inside the crystal (or with the same meaning when a voltage is applied, the crystal deforms elastically). The relationship between polarization and applied stress is linear and given by:

$$\mathbf{P} = \hat{d}\hat{\sigma}$$

where $\mathbf{P}$ is the induced polarization, $\hat{d}$ is the third-rank piezoelectric tensor and $\hat{\sigma}$ is the second-rank stress tensor [8]

2.3.4 Pyroelectric effect

Lithium Niobate is also characterized by the pyroelectric effect: the spontaneous polarization of the material can be modified by varying the temperature. The relationship between the variations of polarization and temperature is linear and given by:

$$\delta\mathbf{P} = \hat{\phi}\delta T$$

where $\delta\mathbf{P}$ is the change in spontaneous polarization, δT is the variation in temperature and $\hat{\phi}$ is the pyroelectric tensor. In LN this effect is related to the movement of Lithium and Niobium atoms with respect to the Oxygen planes and parallel to the $\hat{c}$-axis. The i-component of pyroelectric tensor has the following form:

$$\phi_i = \begin{bmatrix} 0 \\ 0 \\ \phi_3 \end{bmatrix}$$

where ϕ_3 = -4×10^{-5} C $K^{-1}m^{-2}$. This negative value means that, upon cooling, the face of the crystal +c becomes more positively charged as in normal situation.
As a consequence the pyroelectric field has the following form:

$$E_{pyro} = -\frac{1}{\epsilon\epsilon_0}\frac{\partial P_s}{\partial T}\Delta T k_s$$

where P_s is the spontaneous polarization vector. This field is directly proportional to the variation in temperature and has an opposite orientation with respect to the spontaneous polarization direction k_s.
The pyroelectric field generated in Lithium Niobate can interact with micro-nano droplets and can be exploited to manipulate these droplets thanks to electrophoresis or dielectrophoresis effects [28].

2.3.5 Photovoltaic effect

Lithium Niobate is also characterized by the photovoltaic effect: when the material is illuminated at a specific wavelength, a stationary electric current rises due to the photoexcitation of electrons from the valence band to the conduction band. This effect is related to the fact that Lithium Niobate is a non-centrosimmetryc crystal, which forces the photoexcited charges to move along a preferred direction (parallel to the $\hat{c}$-axis). This effect will be treated in more details in the next sections by considering the specific case of $LiNbO_3$ doped with Iron (giving the specific and most commonly used theoretical model).

2.3.6 Photorefractive effect

The combination of both the electro-optic effect and the photovoltaic effect constitutes the photorefractive effect of Lithium Niobate, which is the modification of the refractive index of the material when exposed to light [29], [30]. This effect is characterized by different stages (shown in Fig. 2.4):

- first the crystal is illuminated with the desired light pattern;
- then the electrons in the illuminated area are photoexcited from the valence band towards the conduction band;

- after that the electrons are transferred inside the material by diffusion, drift phenomena or photovoltaic effect till they are trapped inside acceptors sites. In particular if the electrons are trapped inside the non-illuminated region they cannot be photoexcited anymore. This phenomenon generates a non-uniform charge distribution and an internal space-charge field (E_{sc}) is created.
- The generation of the space-charge field leads to the modification of the refractive index value of the material thanks to the electro-optic effect of Lithium Niobate.

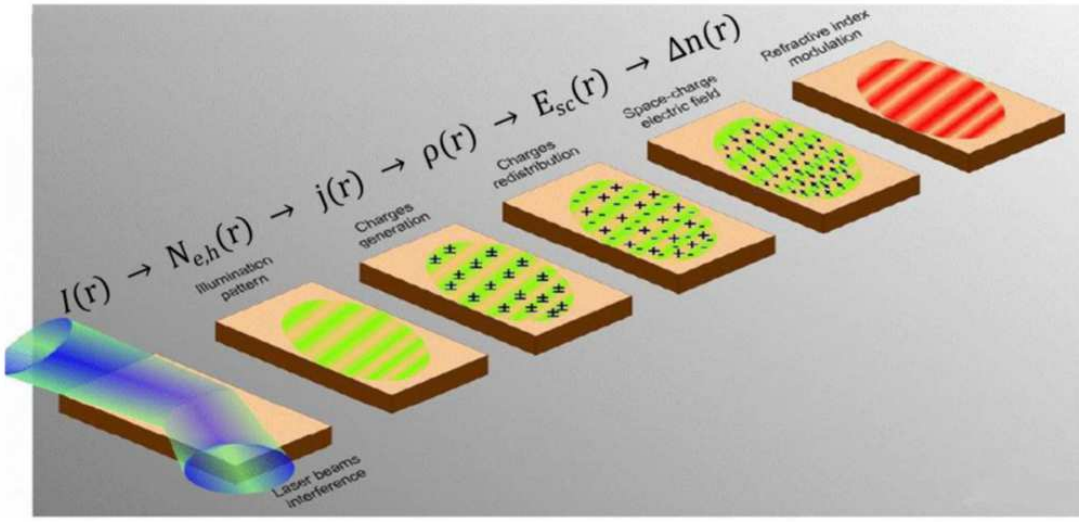

Figure 2.4: Photorefractive effect in $LiNbO_3$ [26].

In case of Lithium Niobate crystals the photorefractive effect is deeply influenced by the impurities present in the material and by the intrinsic antisites Nb ions. In congruent $LiNbO_3$, Niobium antisites ions are present in 2 states: Nb_{Li}^{4+} and Nb_{Li}^{5+}: the pentavalent ions act as acceptors since they trap electrons. After that they transform into Nb_{Li}^{4+} ions, then they can lose an electron thanks to photoexcitation processes coming back to Nb_{Li}^{5+} ions. The space charge field produced in this configuration at saturation can reach values of the order of 10^4-10^5 V m^{-1}. If Lithium Niobate is doped using transition metals such as Iron or Copper, this physical phenomenon can be enhanced and the space charge field at saturation can reach values up to 10^6 V m^{-1}. Doping $LiNbO_3$ with other elements such as Manganese or Zinc can reduce the photovoltaic-photorefractive properties of the material.

2.4 Photovoltaic effect in Lithium Niobate doped with Iron

The photovoltaic current J_{ph} is one of the 3 main contributions, promoting the motion of charge carriers in $LiNbO_3$ when illuminated. The other 2 contributions for the current density are: the drift one J_{drift} related to the presence of an external electric field and the diffusion one J_{diff}. As a consequence the total current density (in general function of spacial coordinates and time) J_{tot} can be written as:

$$J_{tot}(r,t) = J_{drif} + J_{ph} + J_{diff}$$

Moreover both Poisson and continuity equation must be valid:

$$\nabla \cdot (\hat{\eta} E) = \frac{\rho}{\epsilon_0}$$

$$\nabla \cdot J + \frac{\partial \rho}{\partial t} = 0$$

where ρ is the charge density (in general function of both space and time as the current density), $\hat{\epsilon}$ is the dielectric tensor, ϵ_0 is the vacuum dielectric permittivity and E is the total electric field.

2.4.1 Drift current density

The first contribution to total current density is the drift one, related to the motion of charge carriers due to the interaction with an external electric field.The drift density current (J_{drift}), obtained thanks to Ohm's law, can be written as:

$$J_{drift} = q\hat{u}_{e,h}N_{e,h}E$$

$$\hat{\sigma} = q\hat{u}_{e,h}N_{e,h}$$

where $\hat{\sigma}$ is the conductivity tensor, $\hat{u}_{e,h}$ is the mobility tensor for the charge carriers in the material, q is the elementary charge, $N_{e,h}$ is the concentration of charge carriers (electrons or holes). In the previous formula is the total electric field and in the case of Lithium Niobate it can be given by the sum of 3 different contributions: the external electric field (E_0), the field related to the pyroelectric effect (E_{pyro}) and the space charge field (E_{sc}) related to charge redistribution, when the material is exposed to illumination. In the case of LN doped with Iron the pyroelectric contribution is negligible when the illumination intensities are below 10^5-10^6 W m^{-2}.

2.4.2 Photovoltaic current density

The photovoltaic density current (J_{phv}), and in particular its i-component, is given by:

$$J_{phv,i} = \beta_{ijk}e_j e_k I \qquad\qquad i,j,k = 1,2,3$$

where β_{ijk} are the components of the complex photovoltaic tensor, e_j and e_k are the electric field unitary vectors and I is the illumination intensity.
In the case of a linearly polarised wave, the real part of $\beta_{i,j,k}$ is sufficient to describe this kind of wave; instead in the case of a circularly polarised wave the imaginary part of the photovoltaic tensor is needed too. In the case of LN, the photovoltaic tensor has four independent non null components: β_{333}, β_{311}, β_{222} and β_{113}.
This density current contribution is related to the fact that photoexcited electrons have a preferential moving direction (parallel to the $\hat{c}$-axis because $LiNbO_3$ is a non-centrosymmetric material. So in LN the z-component of the photovoltaic current density is the dominant one, while the other 2 components parallel to the $\hat{x}$ and $\hat{y}$ axes are about one order of magnitude lower.
The photovoltaic density current can be described in an alternative way using the following mathematical expression:

$$J_{phv,i} = K_G \alpha I = \alpha \frac{\mu \tau_{ph} E_{ph}}{h\nu} I$$

where K_G is the Glass constant, which is equal to 2.8 $\times$ 10^{-11} m V^{-1} for Lithium Niobate doped with Iron, α is the absorption coefficient, μ is the mobility of charge carriers, τ_{ph} is the characteristic time for photovoltaic process and h$\ni$ is the energy of the photons belonging to incident radiation.
The absorption coefficient can be written in the following form:

$$\alpha = s_{Fe^{2+}}[Fe^{2+}]$$

where $s_{Fe^{2+}}$ is the absorption cross-section of Fe^{2+} ions and $[Fe^{2+}]$ is their concentration.

2.4.3 Diffusion current density

The diffusion density current (J_{diff}), related to presence of a charge concentration gradient inside $LiNbO_3$, is given in module by:

$$J_{diff} = -q\hat{D}\nabla N_{e,h}$$

$$\hat{D} = \frac{\hat{\mu_{e,h}} K_B T}{q}$$

where $\hat{D}$ is the diffusion tensor, q is the elementary charge, K_B is the Boltzmann constant and T is the absolute temperature.

2.5 One-center Charge Transport Model

In general the photovoltaic effect in Lithium Niobate is enhanced by doping the material with transition metals and the most commonly used dopant material is Iron. In this configuration iron ions appear in 2 valence states: Fe^{2+} and Fe^{3+} acting respectively as donors and acceptors of charge carriers (electrons in particular). The process is the described with the following relationship (and the process is shown in Fig. 2.5):

$$Fe^{2+} + h\nu \longleftrightarrow Fe^{3+} + e^-$$

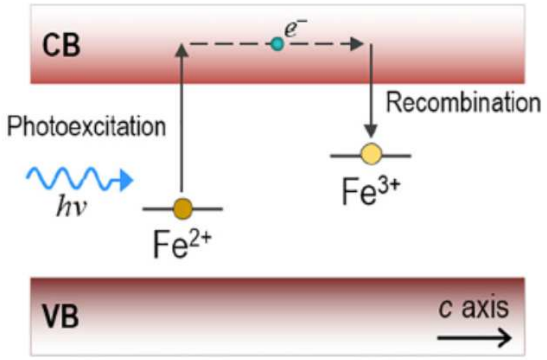

Figure 2.5: Mechanism of the transport of photoexcited electrons in $LiNbO_3$ doped with Iron [31].

The easiest and most used physical model in order to describe the photovoltaic effect in Lithium Niobate doped with iron is called one charge center transport model: this model is based on a set of rate equations derived by Vinetskii and Kukhtarev and is valid for intensities lower than 10^6 W m^{-2} [32]. This model expects that only one kind of ions influences the photovoltaic effect (here the origin for the name of the model) and in the range of intensities considered the dominant contribution is related to Fe dopants. Over the threshold value of 10^6 W m^{-2}, the contribution of Nb antisites ions starts to become non negligible.
The variation of the number of charge carriers (the electron concentration in the conduction band or holes in the valence band) in the Lithium Niobate crystal is given by the following expression:

$$\frac{\partial N_e}{\partial t} = (sI + \beta_t)N_{Fe^{2+}} - \gamma_{e,h}N_{e,h}N_{Fe^{3+}} - \frac{\nabla \cdot J_{tot}}{q}$$

where q and $N_{e,h}$ are respectively the elementary charge and the electron carrier concentration, s is the photoionization cross-section, $\gamma_{e,h}$ is the recombination constant and β_T is the coefficient of thermal generation. Moreover the 2 following relations for the variations in time of the concentrations $N_{Fe^{2+}}$ and $N_{Fe^{3+}}$ hold in module:

$$\frac{\partial N_{Fe^{2+}}}{\partial t} = -\frac{\partial N_{Fe^{3+}}}{\partial t} = -(sI + \beta_t)N_{Fe^{2+}} + \gamma_e N_{e,h} N_{Fe^{3+}}$$

$$j = j_{drift} + j_{phv} + j_{diff} = q\hat{u}_{e,h} N_{e,h} E + sIK_G N_{Fe^{2+}} - q\hat{D}\nabla N_{e,h}$$

where $\hat{u_{e,h}}$ is the mobility tensor of the charge carriers, $\hat{D}$ is the diffusion tensor, β_t is the thermal generation rate, T is the absolute temperature, K_G is the Glass constant, I is the illumination intensity, s is the photoabsorption cross-section and E is the electric field inside Lithium niobate crystal, that is characterized by the sum of the external electric field E_0 and the space charge field E_{sc}, neglecting the pyroelectric contribution.
Furthermore the Poisson equation and the the continuity equation for charge conservation can be written in the following forms:

$$\nabla \cdot (\hat{\epsilon}\epsilon_0 E_{sc}) = \rho = q(N_{e,h} + N_{Fe^{2+}} - N_{Fe^{2+}}(0))$$

$$\nabla \cdot j = -q\frac{\partial N_{Fe^{2+}}}{\partial t} - q\frac{\partial N_{e,h}}{\partial t}$$

where $N_{Fe^{2+}}(0)$ is the initial concentration for donor ions in absence of illumination of the sample.
Assuming $N_{e,h} << N_{Fe^{2+}}$, in the first equation $N_{e,h}$ can be discarded. Moreover using the adiabatic approximation, assuming that the transition from the initial state to the state of quasi-equilibrium is very fast, it's possible to derive:

$$N_{e,h}(r,t) = \frac{sI + \beta_T}{\gamma_{e,h}} \frac{N_{Fe^{2+}}(r,t)}{N_{Fe^{3+}}(r,t)}$$

Instead from the definition of electric conductivity, it's possible to derive:

$$\sigma = \frac{q\mu sI}{\gamma_{e,h}} \frac{N_{Fe^{2+}}}{N_{Fe^{3+}}} + \frac{q\mu\beta_T}{\gamma_{e,h}} \frac{N_{Fe^{2+}}}{N_{Fe^{3+}}} = \sigma_{ph} + \sigma_{dark}$$

where σ_{ph} is called photoconductivity and is directly proportional to the illumination intensity; instead σ_{dark} is called dark photoconductivity and depends on the coefficient of thermal excitation of electrons in absence of illumination. Moreover both σ_{ph} and σ_{dark} depend on the reduction degree (R) of the Iron dopant:

$$R = \frac{N_{Fe^{2+}}}{N_{Fe^{3+}}} = \frac{[Fe^{2+}]}{[Fe^{3+}]}$$

So the reduction degree is nothing but the ratio between the concentrations of donor and acceptors ions in $LiNbO^3$ doped with Iron.
Assuming a null external electric field and that the field related to the photovoltaic effect is dominant over the contribution related to diffusion, it's possible to describe the space charge electric field with the following mathematical expression:

$$E_{sc} = E_{sc}^{sat}(1 - e^{-t/\tau_{sc}})$$

where E_{sc}^{sat} is the saturation value of the electric field joined during the process and τ_{sc} is the characteristic constant time, that governs the exponential behaviour of the space charge field

inside Lithium Niobate doped Iron crystals.
Furthermore the following relationships hold:

$$\tau = \frac{\epsilon_{33}\epsilon_0}{\sigma_{ph}} = \frac{\epsilon_{33}\epsilon_0\gamma}{e\mu sI}\frac{[Fe^{3+}]}{[Fe^{2+}]}$$

$$E_{sc}^{sat} = \frac{K_G\gamma}{e\mu}[Fe^{3+}]$$

From the 2 previous equations it's clear that the characteristic time τ is inversely proportional to the reduction degree of the Iron dopant R and the saturation value of the space charge field is directly proportional to the concentration of Fe acceptors ions $[Fe^{3+}]$. Experimentally the space charge electric field could join values of 10^5-10^6 V m^{-1} inside Lihtium Niobate doped with Iron and is uniform along $\hat{z}$ direction (and so the field is parallel to the $\hat{c}$ axis).

2.6 Optowetting on $LiNbO_3$

One of the main goal of microfluidics is to manipulate droplets over a surface and the most commonly used technique is the electrowetting by tuning the wettability of the surface itself. But electrowetting has 2 main drawbacks: first since fixed metallic electrodes are required for applying the desired voltage difference to the droplet and the substrate, this method isn't characterized by a high degree of reconfigurability and then expensive facilities for the production of the device such as photolitographic techniques for the realization of the sample or the electrical circuits needed for the electrodes are required.
In order to overcome these drawbacks a novel technique has been developed and called optowetting: it consists producing virtual reconfigurable electrodes by illuminating a suitable material with the desired light pattern and then exploits these electrodes to manipulate water droplets or charged particles.
Lithium Niobate is a suitable material in order to develop optowetting: in fact its photovoltaic effect can be exploited to generate virtual reconfigurable electrodes and so, by exploiting them, manipulating the desired objects. As previously described, the doping process of $LiNbO_3$ (in particular using Iron) allows to increase of at least one order of magnitude the photovoltaic electric field with respect to the case of undoped material; as a consequence doped with Iron Lithium Niobate is usually preferred for optowetting applications [33].
The manipulation of micro/nano objects is obtained exploiting the electrophoretict effect (EP) in the case of charged objects (dielectric particles for example) or the dielectrophoretic effect (DEP) in the case of neutral objects (water droplets for example). The expression for the EP and DEP forces acting on a spherical particle are respectively:

$$F_{EP} = qE \qquad\qquad F_{DEP} = (p \cdot \nabla)E$$

where E is the electric field and p is the induced dipolar momentum by the field on the neutral object. The DEP force acting on a spherical water droplet in a not-homogeneous and non-oscillating electric field can be also given by the following relation:

$$F_{DEP} = 2\pi r^3 \epsilon_w \frac{\sigma_w - \sigma_a}{\sigma_w + 2\sigma_a}\nabla(E^2)$$

where r is the diameter of the droplet, E is the electric field, ϵ_w is water dielectric constant, σ_w is the DC conductivity of water and σ_a is the DC conductivity of air. From the previous

formula it's possible to derive an expression for the polarizzability of the neutral object:

$$\alpha_p = 2\pi r^3 \epsilon_w \frac{\sigma_w - \sigma_a}{\sigma_w + 2\sigma_a}$$

. Under the previous hypothesis, the polarizzability α_p becomes a scalar, but in general it's a tensor $\alpha_{p,i,j}$; and the dipole momentum becomes a tensor too. The following tensor relationship holds:

$$p_{i,j} = \alpha_{p,i,j} E_j \qquad\qquad i,j,k = 1,2,3$$

The sign of the dielectrophoretic force depends on the sign of the polarizzability, which depends on the relative difference between the conductivity of the neutral medium and the host medium in turn. If $\sigma_w > \sigma_a$, the neutral object experiences an attractive force; instead the force is repulsive in the opposite case.
In the specific of a water droplet as neutral object and air as hosting medium, since $\sigma_w \sim 5*10^{-6}$ S m^{-1} and $\sigma_a \sim 10^{-9}$ S m^{-1}, the DEP force is greater than zero and the water droplet displays a "positive DEP" and is subjected to an attractive force towards regions where the electric field is characterized by high intensity values.
A model for charge distribution on a z-cut Lithium Niobate sample illuminated with a circular spot in a homogeneous way has been realized by performing some simulations starting from rate equation, controlling the photovoltaic properties of LN [31]. These simulations allow to determine the behaviour of both the electrophoretic forces and potentials acting on charged objects and dielectrophoretic forces and potentials acting on neutral objects instead.
In Fig. 2.6 the results of the simulations for the EP and DEP forces outside a z-cut Lithium Niobate sample illuminated with a single circular spot with homogeneous intensity are shown: these results are not computed, when the electric field generated in LN due to its photovoltaic effect has reached its saturation.

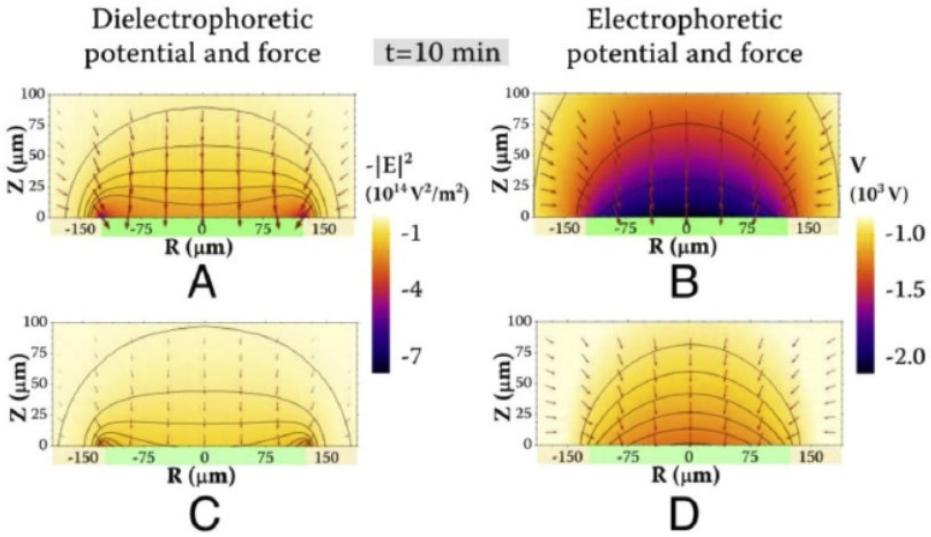

Figure 2.6: (a) and (c) images show the DEP forces and potentials behaviours, while (b) and (d) images show the EP forces and potential behaviours. (a) and (b) corresponds to the illuminated face of the sample, while (c) and (d) correspond to the non-illuminated face. In the four images the arrows indicate the local direction of DEP or EP forces. The green area indicates the extension of the illumination pattern [31]

Observing image (a) and (c) its clear that the dielectrophoretic force is maximum at the border of the illuminated area, minimum in the center and it's perpendicular to the surface above the illuminated region (an experimnetal validation of this phenomenon has been realized by Puerto

A. and others [34]); while the electrophoretic force is minimum at the borders of the illuminated area and maximum at the center (images (b) and (d)). In this simulations the electric field isn't at saturation and for this reason the DEP and EP forces related to the illuminated and non-illuminated faces display different magnitudes. Moreover from the theoretical models it's known that when the illumination time increases, charges tend to accumulate more at the borders of the illuminated area than in the center [31].
Since Lithium Niobate is a solid material, the motion of a water droplet becomes very difficult since the droplet could experience both pinning phenomena at surface defects and a friction force. In order to reduce the effect of the friction force to which a moving body is subjected, it's needed to realize a specific coating over the bare surface of Lithium Niobate, obtaining a liquid-infused surface (LIS). Since a liquid surface is intrinsically smooth down to atomic scale and moreover it's also a defect-free surface in principle, the manipulation of a moving body becomes easier and more reproducible in time.

Chapter 3

Experimental set-up

To perform the optowetting study, the experimental set-up needs to be constituted by 3 main parts: the Lithium Niobate sample, the optical set-up, and the humidity chamber.
The optical part of the set-up needs to be realized so that the LN sample is illuminated with the right intensity so that the photovoltaic effect of the material can be exploited; for this reason, a laser source is required. The laser source needs to be chosen with the right wavelength, matching the absorption range of Lithium Niobate and moreover it needs to be of high power (at least greater than 500 mW). The choice of a laser beam is related to the fact that a laser beam is collimated and it is characterized by a high degree of spatial and temporal coherence and these requirements are fundamental for exploiting the photovoltaic effect of LN. Then the optical path needs to be constituted by a series of lenses and mirrors, that allow to point the laser beam from the source towards the sample and it's important to trying to reduce the losses over the entire path so that the maximum illumination power could join the sample. After that it is needed a component that receives laser light in input and modulates the light in phase so that different illumination patterns (spots, stripes or something more complex) can be created and projected over the sample. Finally one or more cameras are needed in order to record the physical phenomena and to observe the LN sample from different points of view.
The second part of the set-up is the Lithium Niobate sample: it is chosen to use a sample doped with Iron with a certain reduction degree. Then, over the sample a liquid-infused surface (LIS) needs to be realized to avoid droplet pinning over surface defects and favoring their motion. The sample needs to be mounted inside a specific holder and put in a motorized system so that it's possible to move the sample in different directions.
Since almost all the measurements require controlled humidity conditions, a proper humidity chamber is needed to isolate the Lithium Niobate sample from the outside environment. This holder should have the right dimensions with respect to the sample, then it needs to be as closer as possible in order to reduce the interactions with the outside environment. Moreover it should contain one or more regions, where it will be possible the material used to change local humidity around the sample and finally it needs to be constituted by transparent windows so that it will be possible to observe the sample with the chosen cameras.

3.1 Optical set-up

The first part of the experimental set-up is the optical part, that needs to satisfy the previous requirements. An image of the entire optical set-up, starting from the laser source till the LN sample, is shown in Fig. 3.1:

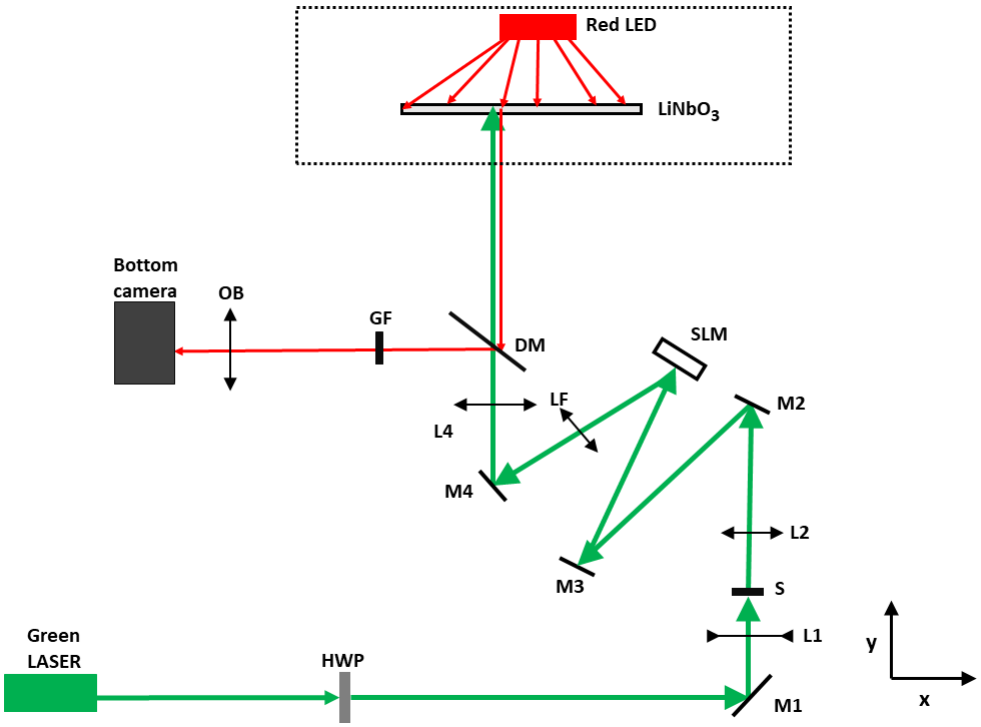

Figure 3.1: Scheme of the optical path with its components. $LiNbO_3$ sample (in the dotted rectangular) is on a different plane with respect to the laser.

Fig. 3.1 shows a schematic view of the optical part of the set-up in the plane (x,y); but in the upper part of the figure there is a dotted rectangular and inside the $LiNbO_3$ sample and the red led are represented. This part of the set-up in the dotted rectangular belongs to another plane (x,z) and it's represented better in Fig. 3.2.
Observing the previous image, the optical part of the set-up is constituted by the following components:

- the laser beam, which is a diode-pumped solid-state laser, emitting in continuous wave. The laser beam emits green light with a characteristic wavelength of 532 nm; moreover the laser beam has a diameter of about 1.5 mm and a maximum nominal power of 1 W.
- 4 mirrors (M1, M2, M3 and M4) are placed in order to control the direction of laser light on the optical line.
- A half-wave plate (**HWP**), placed after the laser source, allows to select the polarization of laser light. This optical component is mounted on a motorized goniometer and it is controlled by the proper software installed on a computer.
- A beam-expander is needed to enlarge the diameter of the beam and it's made of two lenses, the first diverging (**L1**) and the second one converging (**L2**); after the second lens the beam is collimated with a diameter of 8 mm. Between the 2 lenses an optical shutter (**S**) is mounted. The shutter is opened or closed by simply pressing a button and it allows to illuminate or not the sample.
- The spatial light modulator (**SLM**) is needed modulate laser light in phase and then project the desired light pattern on the lithium niobate sample. The outgoing laser light from the SLM hits the Fourier lens (**LF**), which is needed to go back to real space eliminate the zero-th order of the diffraction. Then the converging lens **L4** is necessary to focus laser

light on the $LiNbO_3$ sample. The LN sample is illuminated from bottom by the green laser light.

- Two CCD BAsler acA1300-200um cameras are present in order to record the physical phenomenon: the first one (not shown in Fig. 3.1) allows to obtain a lateral view of the sample. Instead the second one (shown in Fig. 3.1) allows to observe the sample from the bottom (**Bottom camera**). This camera is equipped with an objective (**OB**).

In Fig. 3.2 there are shown both the illumination of the $LiNbO_3$ sample and how it's possible to obtain 2 different views of the sample lateral and bottom. Regarding the illumination, green laser light hits first a dichroic mirror (**DM**) and then another mirror that allows to illuminate the sample properly.
Regarding the 2 different views of the sample: the lateral is obtained by coupling the specific camera (**Lateral camera**) with a **white LED**, that illuminates the sample; this camera is equipped with an objective (**OL**) different from the one mounted on bottom camera. Instead for obtaining the bottom view with the other camera: the $LiNbO_3$ is illuminated from top using a **red led** coupled with a light diffuser; then the red light passes through the sample and it's reflected by the dichroic mirror towards the camera. A green filter (GF in Fig. 3.1) can be mounted in front of this camera (**Bottom camera**) to better observe the image over the screen of a computer. In Fig. 3.2 the direction followed by green light for sample illumination, by white light for obtaining the lateral view of the sample and by red light for obtaining the bottom view of the sample are indicated with proper arrows. Moreover in Fig. 3.1 the optical path followed by red light is shown in the plane (x,y).

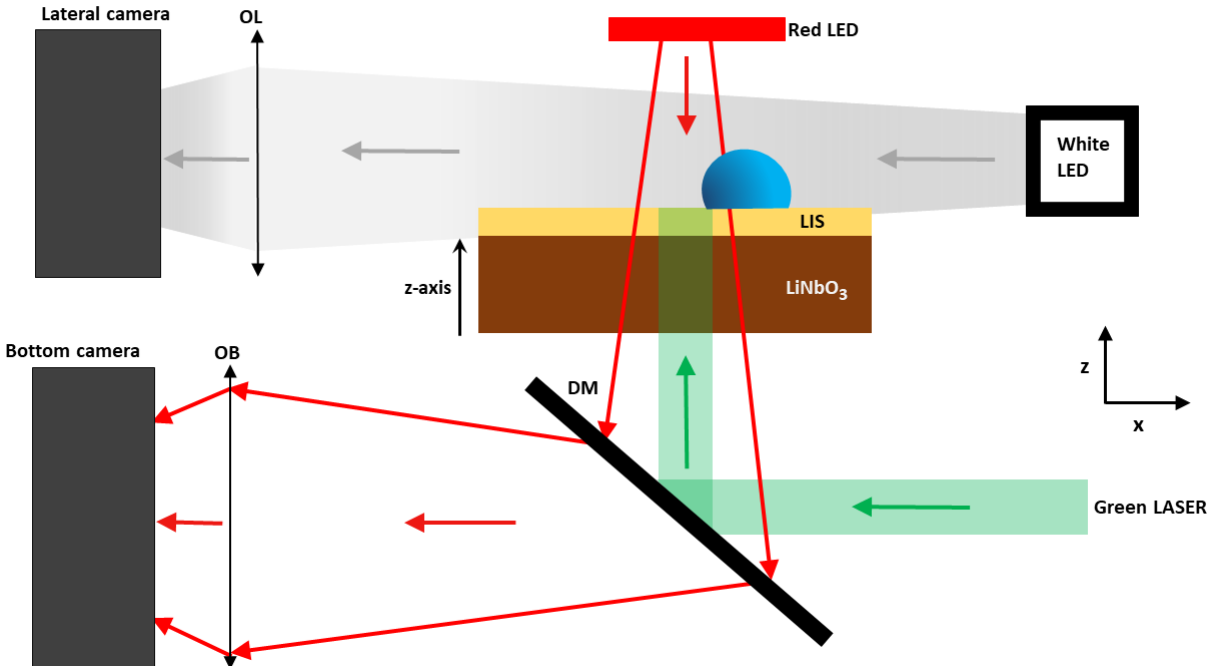

Figure 3.2: Scheme of $LiNbO_3$ sample illumination.

3.2 Spatial light modulator

The illumination of the Lithium Niobate sample is obtained using a Spatial Light Modulator (SLM): it receives laser light in input, then the light is modulated in phase, preserving the amplitude and polarization state, and finally the desired light pattern can be created and used to illuminate the sample.
In particular during the measurements the LCOS-Spatial Light Modulator (liquid crystal on silicon spatial light modulator) is used: it is a SLM based on liquid crystals inside a silicon substrate. The model of SLM used is called SLM Pluto-Nir-011 (shown in Fig. 3.3): it is formed by 2 main components: the driver, needed to control the electronics and coupled to a computer thanks to a DVI/HDMI cable and a chip needed to obtain the actual laser light phase modulation. The chip is composed by different parts: the first one is a silicon substrate that allows to create an electric circuit and receives the instructions from the driver. The second layer of the chip is made of pixel aluminum electrodes to which it is possible to give an electrical potential different one from each other. Between the circuit and the electrodes there are the liquid crystals: first they are horizontally aligned, but when a voltage difference is applied to a certain pixel, the alignment of the crystals is modified. Since liquid crystals display an anisotropic optical behaviour, the refractive index can be modified locally: as a consequence the incoming laser light passing through the crystals modifies its phase and its optical path and globally the shape of the wave-front is changed. The information sent to the driver are given in gray-scale values ranging from 0 to 255.

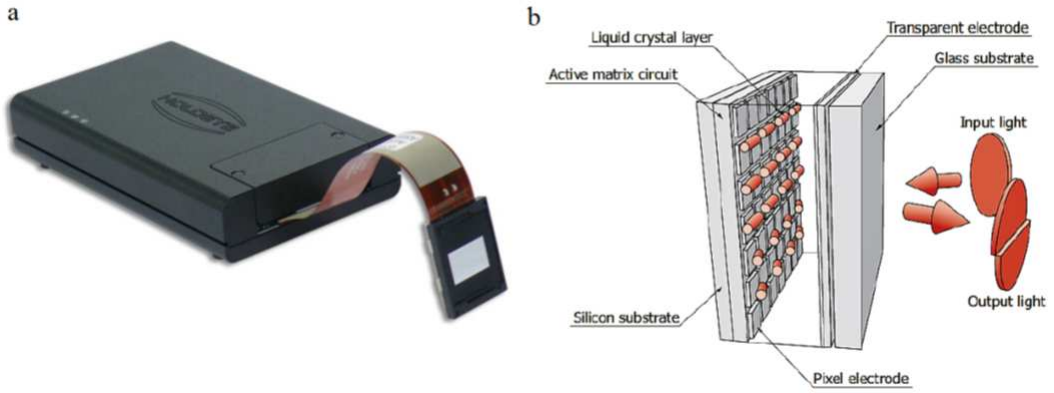

Figure 3.3: (a) The SLM model used during the measurements; (b) internal structure of SLM.

On a PC it's possible to install the control software HOLOEYE SLM pattern generator, which allows to create phase functions, starting from 8-bit images and then it sends the information to the driver of the SLM. One of this specific functions is called diffraction optical element (DOE) and, starting from the input image, it allows to obtain its Fourier transforms with an intensity distribution based on the input image's shape. This phase function is sent to the SLM and the modulation in phase process of input laser light occurs. The connection between the Fourier space, where the DOE operates, and the real space, is obtained thanks to a converging lens (Fourier lens), that receives the light coming from the SLM and allows to create the desired light pattern on the sample with exactly the shape of the input image in the SLM.
In Fig. 3.4: on the left there is an example of input image then sent in the SLM and in grey scale values it represents a white (corresponding to 255 in grey scale) circular spot with 3 mm as diameter with homogeneous intensity inside over a black background (corresponding to 0 in grey scale). Instead on the right there is a screenshot of the DOE function realized by the SLM

driver software.

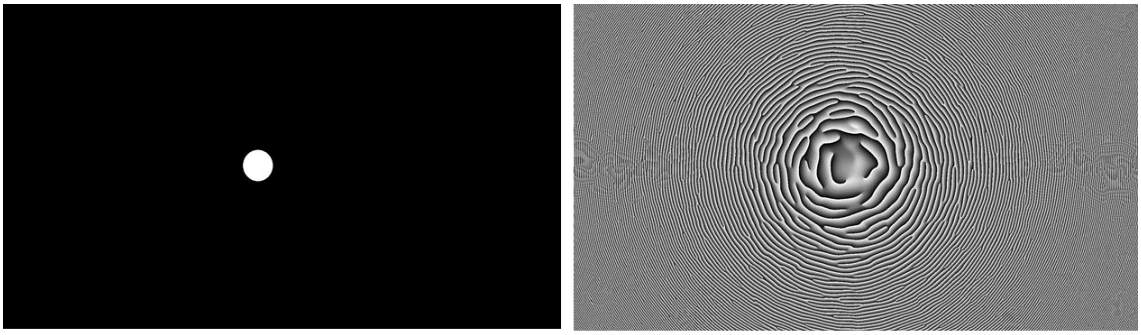

Figure 3.4: On the left original input image sent to the SLM; on the right its DOE function.

3.3 Sample and acquisition system

The sample used during the measurements is a z-cut Lithium Niobate sample doped with Iron at the level of 0.1% mol and a reduction degree R= (32.4± 0.5)% calculated at 532 nm as wavelength with a circular shape with a diameter of 76.2 mm and a thickness of 1 mm. When the measurements are performed the sample is mounted on a specific sample-holder designed with the software Catia V5 and printed using the 3D printer Prusa.
The sample-holder is mounted on a handler, connected to 3 motorized micrometers with a movement range of 25 mm, which allow the motion of the sample in 3 spatial directions (x,y,z) and they can be controlled by the specific software program (PIMikroMove) on the computer. It's also possible to change the angle of the handler using a tilter, that allows a clockwise or counterclockwise with a controlled speed.
The motion of the droplets can be recorded using the 2 different CCD cameras Basler acA1300-200um: the first one is equipped with a Linos objective for the lateral view and it's coupled with the white led. Instead the second camera is equipped with a Navitar MVL7000 objective and allow for a bottom view of the sample. Moreover in order to properly acquire the image with this second camera for bottom view, the sample is illuminated from the top by a red led with a light diffuser put in front of it (Fig. 3.1 and Fig. 3.2); the led has been chosen with a red colour so that new charges are not generated on the LN sample thanks to the photovoltaic effect. For both the cameras it's very important to set carefully the acquisition frame rate in order to record properly the desired physical phenomenon. The videos of droplet motion are saved as sequences of images that can be analyzed after the measurements using a specific software (Image J for example).

3.4 Realization of a Liquid-Infused Surface (LIS)

In order to obtain the motion of droplets, it's necessary to realize a liquid infused surface over the bare surface of $LiNbO_3$ doped with Iron so that droplets could not experience the pinning over surface defects. For the realization of this specific coating, a PTFE filter is used; this filter is unlaminated, chemically and biologically inert and in particular hydrophobic. Moreover the teflon filters are manufactured with a specific process in order to form a high porous, thermostable and with uniform thickness structure. The average roughness and thickness are respectively about 400 nm and about 20 μm.
The choice of using the teflon filter in order to produce the LIS is related to the fact that in

this configuration the filter needs only to be put over the Lithium Niobate sample and then impregnated with specific oil. First the PTFE filter is properly cut according to the shape and dimensions of the LN sample and then it is applied on the sample itself. After that in order to obtain the best adhesion of the filter to the sample, some ethanol is pipetted on the filter and this part of the process ends when the ethanol completely evaporates. Finally the filter needs to be impregnated with specific oil: the choice of the oil is very important since it needs to be "chemical similar" to material of the chosen filter.
Since a teflon filter is used, it needs to be impregnated with a fluorinated oil and in principle 3 different kinds of oil could be exploited: FC-40, Krytox or Fomblin. But FC-40 is characterized by a high vapour pressure, so it evaporates very quickly at room temperature and cannot be used for long-time measurements. Instead the Krytox is more stable than Fc-40, but is the most viscous between the 3 oils so the motion of droplets with small volumes becomes very difficult. For the previously described reasons the teflon filter is impregnated using Fomblin Y lvac 06/6 oil.
In order to have the best possible control of the thickness of the oil layer forming over the porous structure of the filter, the Fomblin oil isn't directly pipetted over the sample. But the impregnation process is obtained by mounting the Lithium Niobate sample coated with the porous PTFE filter on a dip coater. In this process first the sample is completely immersed in a box containing Fomblin oil and then it is removed from the container with a constant velocity. The height (h_0) of the oil layer forming over the porous filter is given by the Landau-Levich law:

$$h_0 = c\frac{(\eta U_0)^{2/3}}{\gamma_{LA}^{1/6}(\rho g)^{1/2}}$$

where η and ρ are respectively the viscosity and density of the oil, γ_{LA} is the surface tension between the oil and the air, c is a constant and U_0 is the withdrawal velocity of the sample from the oil. As a consequence the velocity for which the sample is removed from the oil container strongly affects the thickness of the oil layer forming above the porous surface of the teflon filter. In Fig. 3.5 there is shown then dip coater used for LIS realization is shown: the $LiNbO_3$ sample mounted to the dip coater and ready to be immersed in the box containing oil, which is below the sample itself [35].
In order to obtain the desired LIS a withdrawal velocity of 0.12 mm/min is chosen: in this way, exploiting the Landau-Levich equation, an oil layer with a nominal thickness of 0.5 um is obtained. This specific value for the thickness of the oil layer forming over the substrate is the best one found in previous works in order to obtain a good motion of the droplets without pinning [9]. It's important to notice that this specific value for the thickness of the oil layer has been only computed using the Landau-Levich model, but it has never been effectively measured; one possible measurement technique could be ellipsometry.
An image of the $LiNbO_3$ sample used during measurements, mounted on its specific holder and with the teflon filter applied and impregnated in order to realize the LIS, is shown in Fig. 3.6.

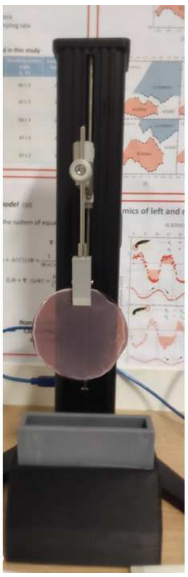

Figure 3.5: The dip coater used for LIS realization with $LiNbO_3$ sample mounted.

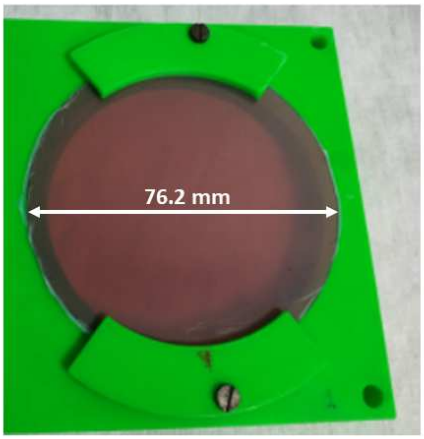

Figure 3.6: Lithium Niobate sample used during the measurements.

3.5 Humidity chamber

The third and last part of the experimental set-up is constituted by the humidity chamber, that is needed to control the humidity around the Lithium Niobate sample, isolating it from the outside environment. This chamber was first projected properly, then designed using the software Catia V5 and finally printed using the 3D printer Prusa. The inner part of this holder is realized so that the Lithium Niobate sample can be mounted and blocked inside; then inside there are two regions, where it's possible to insert the material needed to change humidity around LN sample: when the humidity needs to be increased, some water can be pipetted inside. Instead when it's necessary to reduce the humidity value, a proper quantity of silica stones is used. Moreover this chamber is characterized by the presence of two transparent windows to observe the sample mounted inside.
In Fig. 3.7 the inner part of the humidity box is shown; a Lithium Niobate sample doped with iron is mounted inside and on the left and right parts of the figure it's possible to observe the 2 regions, where the silica stones needed to reduce the humidity around the sample are put. Moreover the 2 transparent windows to observe the sample inside can be seen.
The lid of this holder is characterized by the presence of a hole, where it's possible to put inside the sensor needed to measure the relative humidity around the LN sample. The relative humidity value is obtained thanks to an indirect measurements by using a HIH-4000 Honeywell humidity sensor: this device gives a voltage signal ranging from 0 V to 5 V and thanks to a proper calibration curve (given by the constructor of the sensor), that takes also into account the temperature around the sample, it's possible to obtain the specific humidity value. In Fig. 3.8 the humidity sensor and its calibration curve needed to extract the desired humidity value are shown.
In order to use this sensor, a proper electrical circuit is built: it is pumped at 5 V using an Arduino-Uno case and a resistance of 80 kΩ is mounted between the output pin and the ground. The Arduino-Uno case is put inside a proper holder, designed with the software Catia V5 and then printed using the 3D printer Prusa. In Fig. 3.9 the scheme of the electrical circuit needed to use the humidity sensor and the Arduino-Uno case exploited to pump the circuit built are shown.

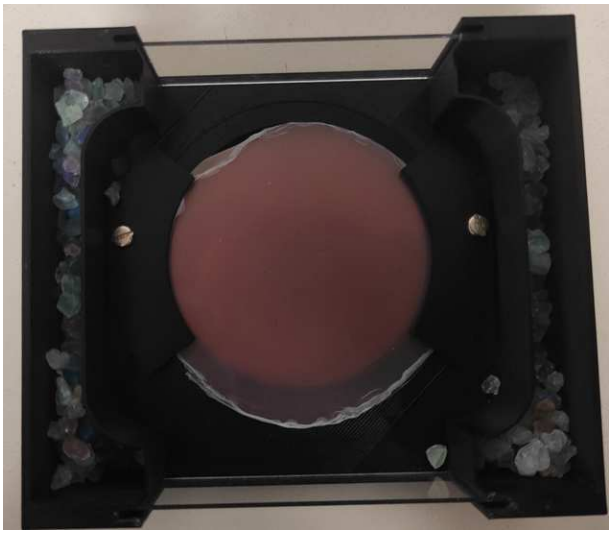

Figure 3.7: Inner part of the humidity chamber; in the regions in the left and right part of the image there are inserted inside the silica stones exploited to reduce humidity around $LiNbO_3$ sample. Two transparent windows for sample observation can be seen.

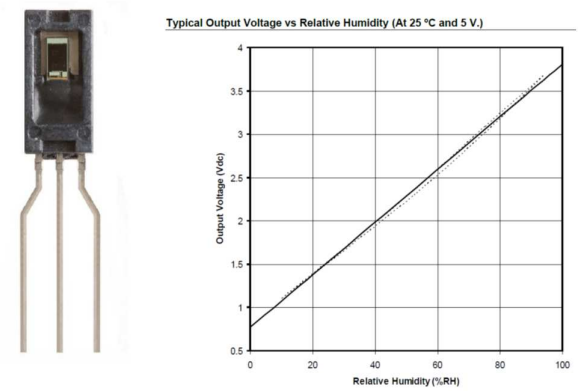

Figure 3.8: On the left one humidity sensor used and on the right the calibration curve to estimate the humidity value.

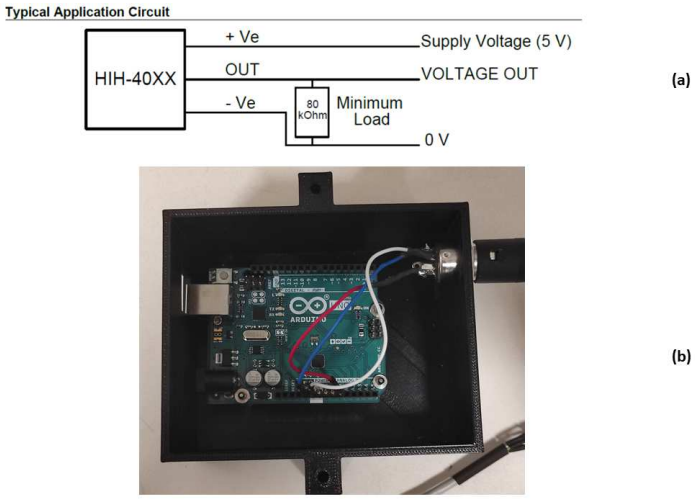

Figure 3.9: (a) Scheme of the electric circuit for the humidity sensor; (b) Arduino-Uno case used to pump the circuit of the humidity sensor.

Chapter 4

Experimental measurements

The experimental measurements belonging to this thesis work are characterized by two main goals that are strictly connected one to each other: the first goal is to elucidate the role of humidity on Lithium Niobate's discharge after the illumination is switched off. The second objective is to control the motion of water droplets on horizontal plane by tuning the local wettability thanks to a suitable illumination of the photorefractive substrate.

4.1 Role of the humidity on the Lithium Niobate discharge

From a theoretical point of view it's well known that Lithium Niobate is characterized by an intrinsic and natural discharge, when the illumination pattern is switched off [26]. Preliminary studies display that some environmental conditions of the laboratory, where the measurements are performed, could affect the photovoltaic properties of LN sample [9]. In particular the attention is focused on the role of humidity over Lithium Niobate discharge: for this reason, the first part of the experimental measurements have the main goal to consider in a qualitative way how humidity could affect Lithium Niobate discharge in different conditions.
Moreover, to the best of our knowledge in literature there are no scientific papers dealing with this topic; as a consequence this part of the thesis work could be considered a sort of pioneering work in trying to characterize more accurately the photovoltaic properties of Lithium Niobate.

4.1.1 Experimental protocol

Regarding the first kind of measurements to investigate the role of humidity, it is important to clarify that is not possible to directly measure the electric field generated by Lithium Niobate after illumination; however it is possible to estimate the role of the humidity on charge accumulation over LN surface using an indirect measurement. It consists in first illuminating a certain region of the sample and then, after having switched off the illumination pattern, generating a pendant water drop on the needle of a vertical syringe pump over the region of the sample previously illuminated. As described in section 2.4 when $LiNbO_3$ is illuminated with proper light, an electric field is generated inside the material due to the photovoltaic effect and this field last also after the end of illumination. In this configuration 2 main forces act on the pendant droplet: the gravitational force and the dielectrophoretic force due to the interaction of the neutral water droplet with the electric field generated in LN. By moving the sample closer and closer towards the needle of the pump, the water droplet experiences a DEP force stronger and stronger. At one point this interaction is so high that the droplet breaks away from the needle of the pump and it falls over the region of LN sample previously illuminated. By fixing some experimental parameters such as power of illuminating laser light, the shape and dimension of the

illumination pattern, the volume of the droplet and the waiting time interval between the end of the illumination and when the pendant droplet is generated, the data and the correspondent trend obtained by measuring the falling distance of the droplet as a function of different values of humidity around the Lithium Niobate sample could give indirect information relatively to the role of humidity on $LiNbO_3$ discharge.
The experimental protocol for this kind of measurements is the following: the Lithium Niobate sample without the LIS coating realized over its surface is mounted inside the humidity chamber and put in a horizontal position; then the humidity working value is chosen and the desired conditions are created inside the box around the LN sample. After about 20-30 minutes the humidity value is stable inside the chamber. A specific point of the LN sample is illuminated with continuous and homogeneous illumination for 1 minute with a circular spot of 3 mm as diameter and a power of 50 mW reaching the sample. Once the illumination is switched off, a specific time interval between the end of the illumination and the generation of a water droplet is waited. After that a pendant droplet of 3 μL as volume is generated over the region of the $LiNbO_3$ sample previously illuminated using a vertical syringe pump; the droplet is generated inside the humidity chamber box thanks to a hole created in the lid of the chamber itself. Then the sample is moved upwards using the specific micromover till the droplet falls towards the sample due to the dielectrophoretic effect. The falling distance is measured starting from the tip of the needle to the surface of the LN sample. For each one of the chosen humidity values at least three different measurements are performed in order to test the experimental reproducibility of the physical phenomenon.
In order to obtain this kind of measurements ultra-pure water with a resistance of 18.2 MΩ is used; moreover three different sets of measurements are performed by changing the waiting time between the end of laser illumination and the instant at which the pendant droplet is generated (and by maintaining fixed all the other experimental parameters: power of the laser, illumination time, illumination light pattern and droplet volume): 30 seconds, 5 minutes and 20 minutes as waiting times are chosen.
In order to perform this kind of measurements it's needed a good alignment between the illuminated region of the $LiNbO_3$ sample and the generated pendant droplet; otherwise if the droplet isn't generated over the proper region, it could happen that it does not feel the effect of the DEP force and it doesn't breaks away from the needle of the syringe pump.
Finally after a certain number of measurements performed using the same LN sample, it is necessary to completely discharge the Lithium Niobate sample: for this reason, water droplets are pipetted over the entire area of the sample and are removed after having waited at least 10-15 minutes. After that to make sure the sample is completely discharged, a pendant droplet is generated again and if it breaks away from the needle of the pump at exact contact of the LN sample, this means the sample is completely discharged.

4.1.2 Pendant drop measurements: results

In Fig. 4.1 a visual example of the measurements performed is shown: h in mm is defined as the falling distance to be measured by varying the humidity around $LiNbO_3$ sample); the green arrow indicates the illumination of the sample from bottom and the red arrow indicates the motion of the water pendant droplet from the needle of the pump towards the sample. In the bottom part of the figure there is a plot of intensity ($I(x)$) as a function of the spacial coordinate (x) in x-direction, that indicates that the illumination of the sample is homogeneous.

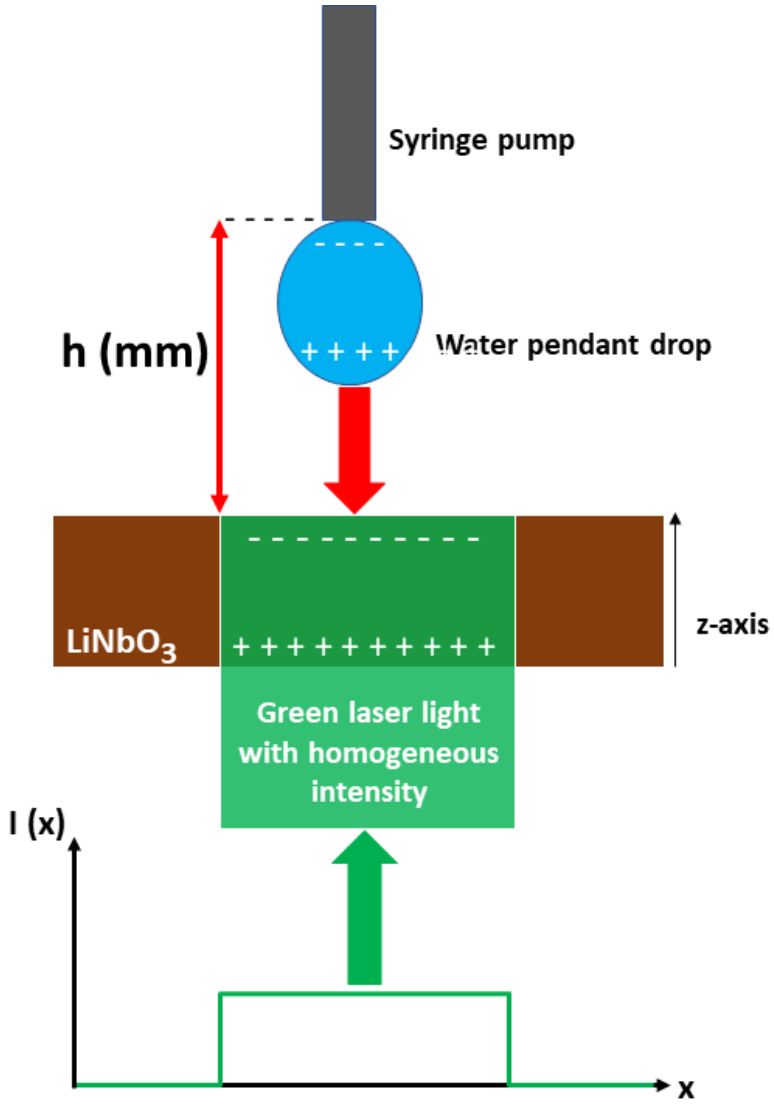

Figure 4.1: Example of measurements performed to study the role of humidity on $LiNbO_3$ discharge. In the bottom part a graph of illumination ($I((x))$ vs x spatial coordinate to indicate the sample illumination is homogeneous

In graph in Fig. 4.2 the falling distance values (h referring to Fig. 4.1) as function of humidity around Lithium Niobate sample are shown by including 3 different data-set related to 3 different waiting times chosen. Moreover in the graph a dashed line is represented: it corresponds to the length of the pendant droplet measured in absence of illumination. So the 3 μL pendant droplet is generated and attached to the needle of the syringe pump; then the $LiNbO_3$ sample is moved upwards till it becomes in contact with the pendant droplet itself and then the desired length

is measured and it is equal to 1.8 mm. If one or more data points fall on this dashed line, it means that for these measurements the specific sample regions, previously illuminated and then over that the pendant droplet is generated, are basically discharged by the humidity around the $LiNbO_3$ sample considered.

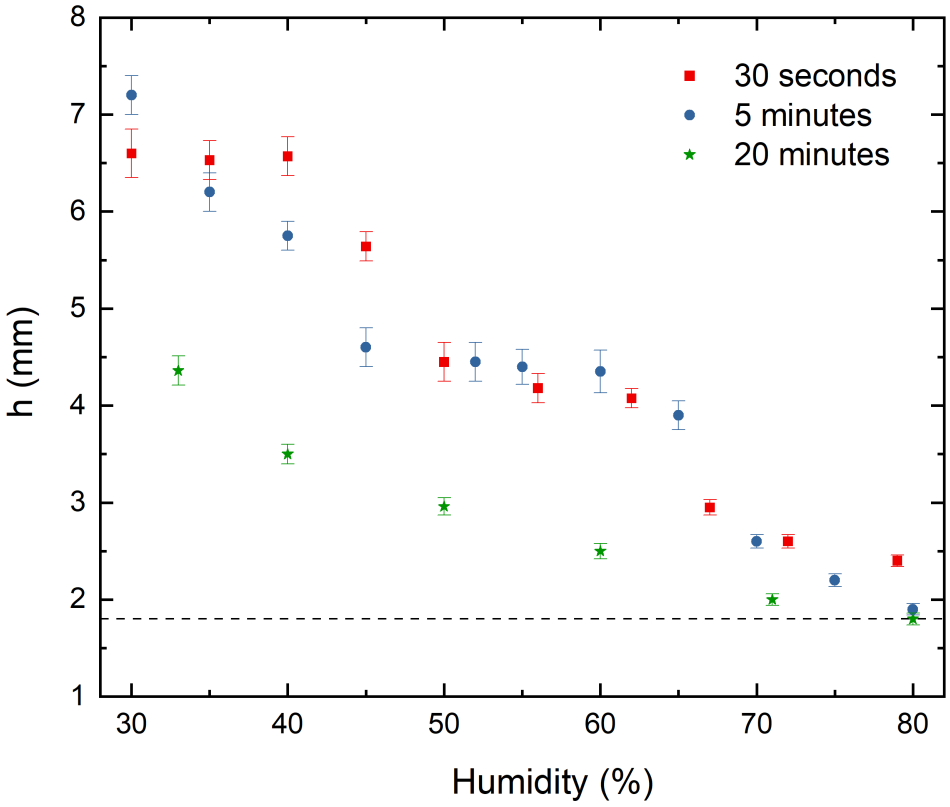

Figure 4.2: Falling distance (h) values as function of humidity around Lithium Niobate sample for 3 different data-set, in which the waiting time is changed.

Observing the plot in Fig. 4.2 some considerations can be performed: in each one of the 3 data set acquired varying between 30% and 80% of humidity values (which is the standard humidity range found in the laboratory), the falling distance (h) decreases by increasing the humidity around Lithium Niobate sample. This specific trend is completely monotonically decreasing in the case of 20 minutes as waiting time; instead for the other 2 trends there is a monotonically decreasing behaviour from 30% to 45% and from 65% to 80% as humidity values. In the middle between this humidity ranges there is a sort of plateaux in the falling distance values as a function of humidity, while it should be expected a completely monotonically decreasing behaviour starting from the lowest humidity value 30% and reaching the higher one 80%. Although the presence of these unexpected plateaux, in general since the falling distance decreases while the humidity around the Lithium Niobate sample increases and having maintaining fixed all the other experimental parameters in each one of the three data-set acquired, the measurements displays in an indirect way that humidity has an important role in promoting the discharge of Lithium Niobate. In particular at 80% of humidity the lithium Niobate sample is completely discharged considering the data acquired with 5 and 20 minutes as waiting times and since the

falling distance value corresponds to the droplet length in absence of illumination (1.8 mm on the dashed line).
Moreover, observing the previous plot, the data acquired at 30 seconds and 5 minutes as waiting times show both the same trend and in the plateaux region by fixing the humidity value the falling distance values are practically equal. Instead there is a great gap between the data acquired with 20 minutes as waiting time and the other two data set; this jump is simply explicable considering the intrinsic discharge of Lithium Niobate.
This measurements are necessary to choose the range of humidity values, in which all the following measurements (regarding droplet motion) will be performed. Observing Fig. 4.2, it's clear that the role of humidity has a less impact over Lithium Niobate discharge in the range between 30% and about 45% as relative humidity around the $LiNbO_3$ sample by considering 30 seconds or 5 minutes as waiting times. For this reason the following measurements are performed in controlled environmental conditions by working in the humidity range between 30% and 40%.

4.2 Study of droplet motion

The second part of experimental measurements is mainly devoted to trying to put in motion and then control water droplets over the surface of $LiNbO_3$ coated with the LIS. First the liquid infused surface allows to drastically reduce the friction force acting on the droplet with respect to the case of moving over the solid surface of LN and moreover the pinning of droplets over surface defects practically disappears. Then the motion of a droplet over a surface could be achieved in 2 different ways:

- in a passive way by tilting the sample considered and in this way the effect of gravity plays in important role in droplet motion;
- or in an active way, where in this case the sample is maintained in a perfect horizontal position and gravity doesn't affect droplet motion.

In previous thesis works [9], [36] the droplet motion was obtained in a passive way, by tilting the sample, but in this work for the following measurements the manipulation of water droplets is achieved in an active way. In particular since gravity does not play a role in droplet motion, the dielectrophoretic interaction between the neutral water droplet and the electric field rising due to LN sample illumination becomes very relevant and it is exploited to put in motion and then control the dynamics of the droplet itself.

4.2.1 Attraction: response time vs illumination power

The first phenomenon studied is the attraction of a water droplet towards a specific illuminated region of the LN sample.
As a first step it's studied how the response time of the droplet to attraction changes by varying the laser power used to illuminate the sample. In this case as "response time" it means the exact time instant at which the droplet feels the attraction towards the illumination pattern due to the dielectrophoretic effect. In this kind of measurements the droplet starts to feel an attraction effect, but it's not sure that in all the measurements the drop moves towards the illumination pattern, covering a part of the illuminated area itself; in fact in some cases (in particular for the data acquired at low powers, which means lower than about 60 mW) the droplet simply feels an attraction, but it doesn't move from its initial position and then it's repelled away far from the illumination pattern.
The experimental procedure to perform the previously described measurements is the following:

first the ultra-pure water droplet is put in the proper position over the Lithium niobate sample thanks to a micropipette; then the main parameters of the illumination pattern (shape of the pattern, dimensions and power of the laser source) are set; after that the sample is illuminated and finally the video recording and acquisition starts. For this measurements the LN sample is illuminated, creating a circular spot with diameter of 3 mm thanks to the SLM, and the illumination process is continuous in time and homogeneous over the surface of the chosen region. The illumination power varies from 20 mW to 180 mW, the maximum possible power value reaching the sample and all the power values are measured at the sample position. The droplet volumes chosen are 3 μL, 5 μL, 7 μL and 9 μL: the choice of this volume range is due to the fact preliminary studies displayed it was very difficult to move droplets with volumes greater than 10 μL. Furthermore regarding droplets with volume lower than 1 μL, they were easier to put in motion, but it was very difficult to control their dynamics along time and along space after the process began. The water droplet is put in a position so that its meniscus is approximately in contact with the border of the circular spot chosen as illumination pattern. Regarding the video acquisition, for all this kind of measurements the Basler camera equipped with Linos objective, needed for the lateral view of the sample is used; for each one of the acquisitions the "instant zero" of the video recordings corresponds to the exact moment at which the illumination of Lithium Niobate sample begins.
In this kind of measurements some practical aspects are crucial: first the droplets needs to put in exact contact with the border of the illuminated region otherwise it could be a wrong estimation of the response time. Then the acquisition frame rate set on the camera becomes crucial because, if wrong, the number of frames acquired could not be enough both to observe properly the phenomenon and to compute the response time correctly. As a consequence since the dynamics of attraction for power values greater than about 100 mW is quite fast, the acquisition frame rate for these measurements is at least doubled with respect to the frame rate for the measurements with illumination power below 100 mW.
Finally the main source of error for the computation of the response time comes from the choice of the exact frame at which the droplet starts to feel an attraction toward the illuminated area. In all the measurements it's important to clarify that in the choice of the correct frame the doubts arose when it was needed to choose between the frame, that after it will be exploited to compute the response time, and one frame more in time or one frame less in time. In order to reduce as much as possible this kind of doubts and possible mistakes, it was also decided to increase the acquisition frame rate in the case of measurements performed at high illumination power values reaching the sample.
In Fig. 4.3 there is a sequence of frames, showing an example of attraction measurement: the droplet volume is 3 μL and the illumination power is 180 mW.

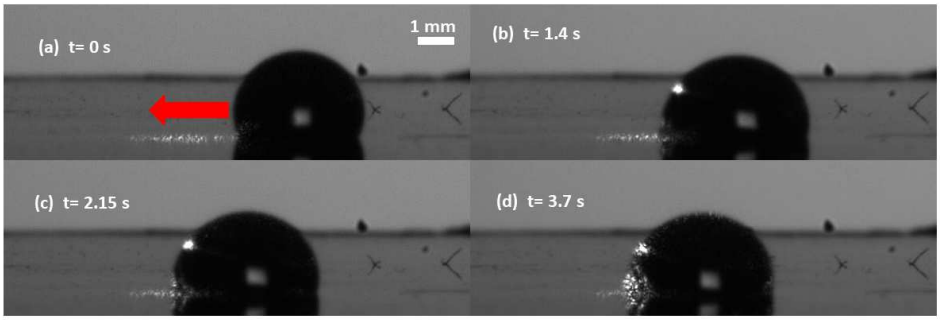

Figure 4.3: Sequence of frames showing an attraction measurement.

In the plot in Fig. 4.4 the data related to response time (indicated with τ_R) for the attraction of a droplet as a function of the laser illumination power (indicated with P) are shown for droplets of different volumes (in the graph legend V indicates the volume of the droplet and d is the characteristic length of the droplet itself).

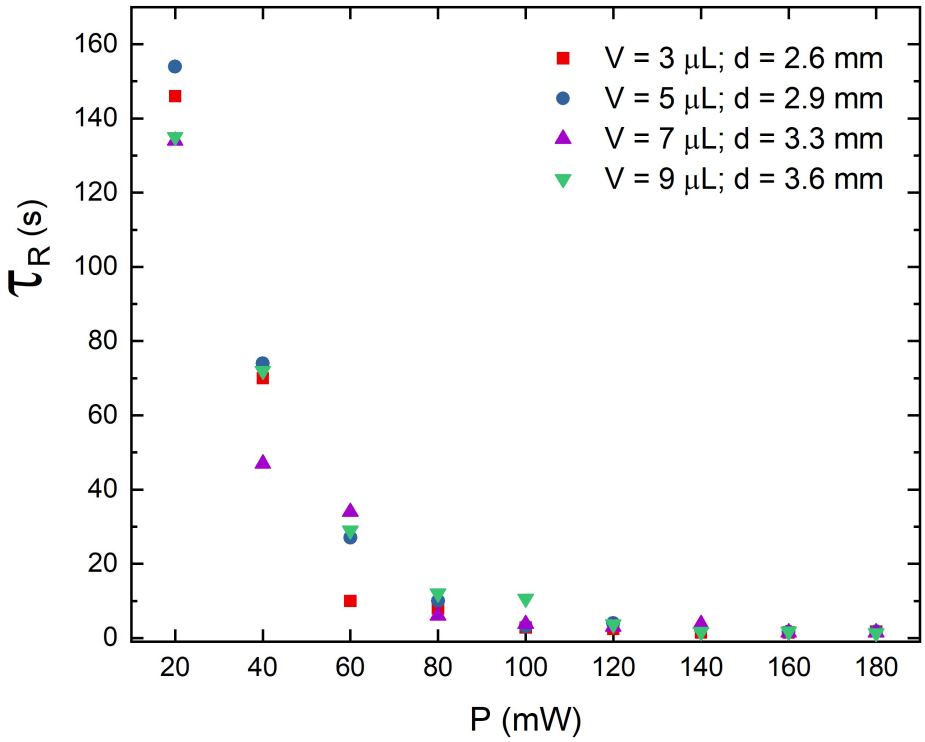

Figure 4.4: Response time (τ_R as function of illumination power P for droplets of different volumes.

Observing the previous plot 2 main conclusions can be extrapolated: first, as one could expect, increasing the illumination power reaching the sample the response time drastically reduces from about 150 s (computed for 20 mW as power) to about 2 s (computed for power values greater than 140 mW). Moreover for illumination power values greater than 120 mW the response time trend seems to display a sort of saturation since the time fluctuations are practically negligible. The second important observation is that the response time for the attraction becomes independent from the droplet volume for power values greater than 80 mW. This characteristic behaviour can be noticed also in some cases, when the illumination power reaching the sample doesn't overcome 60 mW, but in some power regimes the fluctuations in response time are more evident.

4.2.2 Attraction: response time vs mutual distance droplet-illumination pattern

The second goal of this kind of measurements is devoted to study how the response time for attraction changes by varying the mutual distance between the illumination region of the Lithium Niobate sample and the water droplet. In these measurements the sample is illuminated continuously in time and homogeneously in space and the water droplet is put on the sample by increasing the mutual distance between the border of the illumination pattern and the droplet meniscus from one measurement to the subsequent one. In Fig. 4.5 there is a visual scheme of the measurements, showing both the illumination pattern (green circular spot) and the water droplet, where d indicates its characteristic dimension. Moreover the mutual distance (indi-

cated with w) connecting pattern and droplet is put in evidence. As in the previous set of

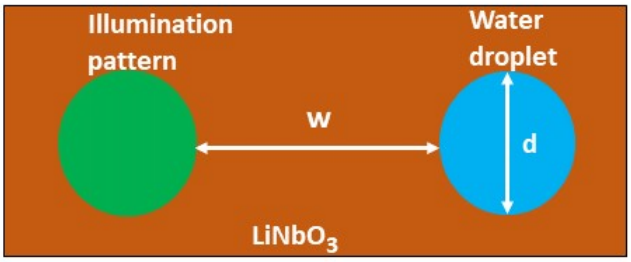

Figure 4.5: Scheme for the measurements in which the response time varies as a function of the mutual distance between illumination pattern and water droplet.

measurements the exact time instant at which the droplet starts to feel the attraction towards the illumination pattern due to the dielectrophoretic effect is computed, although in almost all the cases the droplet isn't put in motion and then covers a region of the illumination pattern. In this case the illumination pattern chosen is again a circular spot with 3 mm as diameter; in one specific set of measurements the power of the laser reaching the sample is maintained fixed, while the mutual distance droplet-pattern varies. In particular 3 different data set are acquired each one for a specific value of laser power: 60 mW, 100 mW and 180 mW. Moreover different set of measurements are performed by changing the droplet volume, which still varies between 3 μL, 5 μL, 7 μL and 9 μL; the video recording is obtained again using the Basler camera equipped with the Linos objective, that allows a lateral view of the sample. Fig. 4.6, Fig. 4.7 and Fig. 4.8 show how the response time (indicated with τ_R) changes as a function of mutual distance (indicated with w) drop-pattern for different illumination powers.

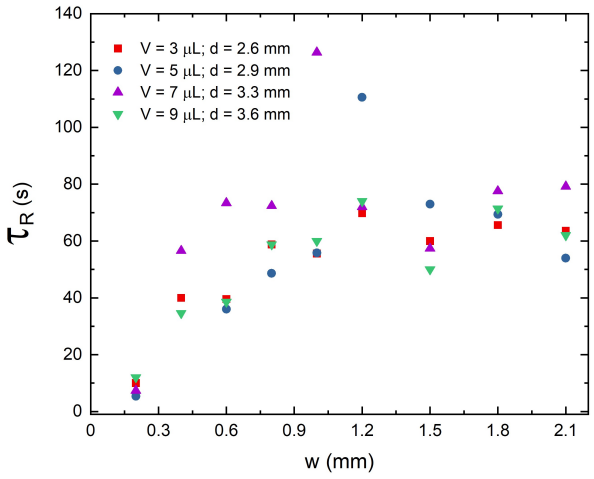

Figure 4.6: Response time (τ_R)) as a function of the mutual distance (w) droplet-illumination pattern for droplet of different volumes and illumination power equal at 60 mW.

Observing the previous 3 plots, some conclusions can be extrapolated: first as expected the response time for attraction increases as the mutual distance droplet-illumination pattern becomes greater. This trend is really clear in the case of illumination power values reaching the sample equal to 100 mW and 180 mW; instead for illumination power value equal to 60 mW this particular behaviour could be observed partly, although there are more oscillations in the response time values with respect to the other two cases (100 mW and 180 mW as power values). Then as in the first type of attraction measurements, it seems the response time is independent

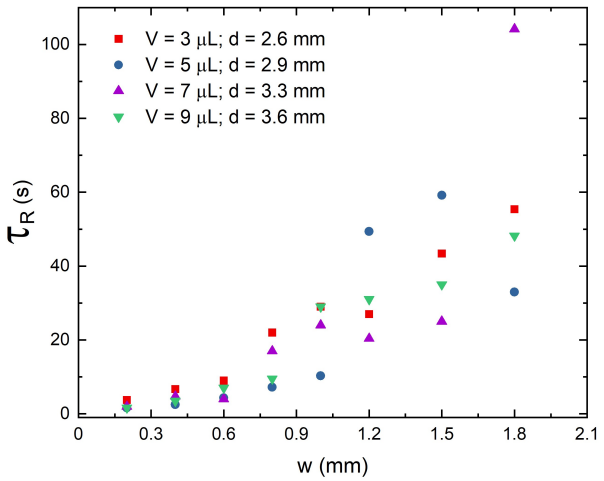

Figure 4.7: response time (τ_R)) as a function of the mutual distance (w) droplet-illumination pattern for droplet of different volumes and illumination power equal at 100 mW.

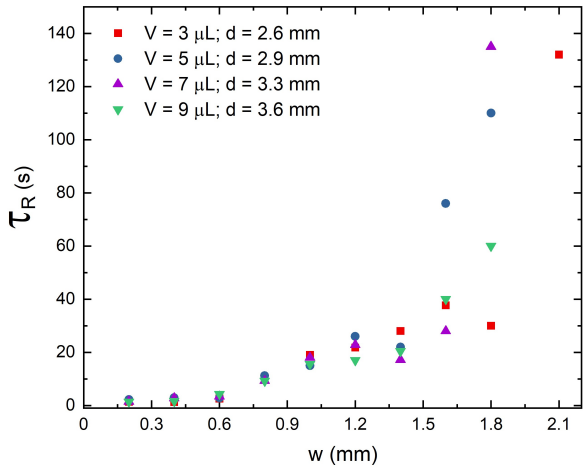

Figure 4.8: Response time (τ_R)) as a function of the mutual distance (w) droplet-illumination pattern for droplet of different volumes and illumination power equal at 180 mW.

on the droplet volume in some situations: in the case of the maximum illumination power value reaching the sample (180 mW) till to 1.4 mm as distance between the droplet and the edge of the of the illumination pattern the response time is practically not dependent by the droplet volumes considered. Instead in the case of 100 mW as power illumination value, this independence of response time from droplet volume holds till 0.6 mm as distance droplet-illumination pattern; finally in the case of 60 mW as illumination power, this specific behaviour of response time occurs only at 0.2 mm of distance between the droplet and the illuminated area.

4.2.3 Attraction: stopping time vs illumination power

In the last part of the attraction measurement we want to put a droplet in motion towards the illuminated region of the $LiNbO_3$ sample and the stopping time is measured as function of different experimental parameters. Regarding the realization of the each measurement first the droplet meniscus is put in contact with the border of the illuminated region in the most accurate possible way; then after the illumination of the sample is switched on, the droplet starts

to move towards the illuminated region due to the DEP effect, covering a specific region of the illuminated area. A time interval (the stopping time properly) passes between the beginning of the illumination and the instant at which the droplet stops its motion over the illuminated area; finally the droplet could be repelled way in a specific direction.
The measurements are realized by putting the water droplet in close contact with the border of the illumination pattern (the illumination of the sample is continuous in time and homogeneous over the surface of the illuminated area again): different set of data are recorded by varying the droplet volume between 3 μL, 5 μL, 7 μL and 9 μL. Furthermore the illumination pattern is changed: in all the cases the shape of the pattern is a circular spot, but the diameter value changes between 3 mm, 1.1 mm, 0.8 mm and 0.5 mm. For each one of these circular spots 3 measurements are performed by choosing 3 specific values for laser power reaching the $LiNbO_3$ sample: 60 mW, 100 mW and 180 mW; finally the video acquisition is obtained thanks to the camera for lateral view of the sample.
In the following there are 2 example plots for these kind of measurements, showing how the stopping time (indicated with τ_S) changes by varying the illumination power (indicated with P). In Fig. 4.9 the droplet volume is fixed to 5 μL and the diameter of the illumination pattern (a circular spot) changes; instead in Fig. 4.10 the spot diameter is maintained fixed and equal to 1.1 mm, while the droplet volume changes in the chosen range.

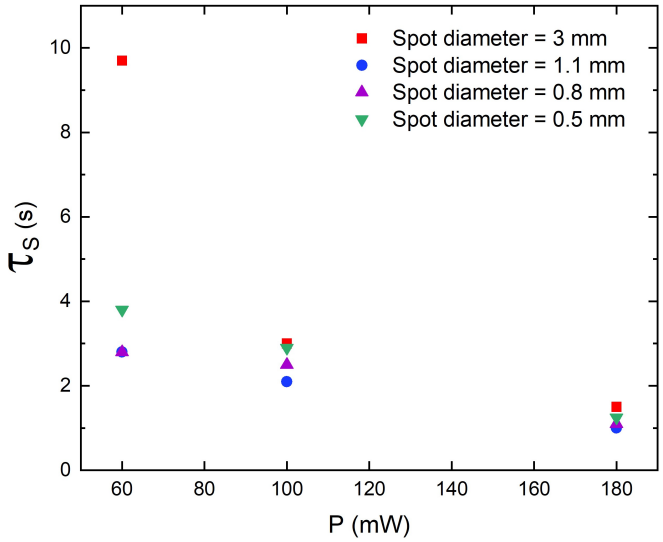

Figure 4.9: First example plot of how the stopping time (τ_S) changes as a function of the illumination power (P). The droplet volume is fixed to 5 μL and the spot diameter changes.

Observing the 2 example plots, some conclusions can be extrapolated: first in almost all cases the stopping time decreases by increasing the illumination power reaching the sample from the lower value 60 mW to the maximum possible one 180 mW. Then the for illumination power values greater than 100 mW the stopping time behaviour seems to be independent on droplet volume, when the spot diameter is fixed at 1.1 mm (Fig. 4.10) or independent on the spot size, when the droplet volume is fixed (to 5 μL in Fig. 4.9). Instead at low power values (60 mW in the example) the stopping time is characterized by non-negligible fluctuations in both cases. Moreover, observing Fig. 4.10, the dynamics of the stopping time (when the spot size is equal to 1.1 mm) is quite fast for each one of the 3 illumination power values chosen and it's of the order of few seconds.

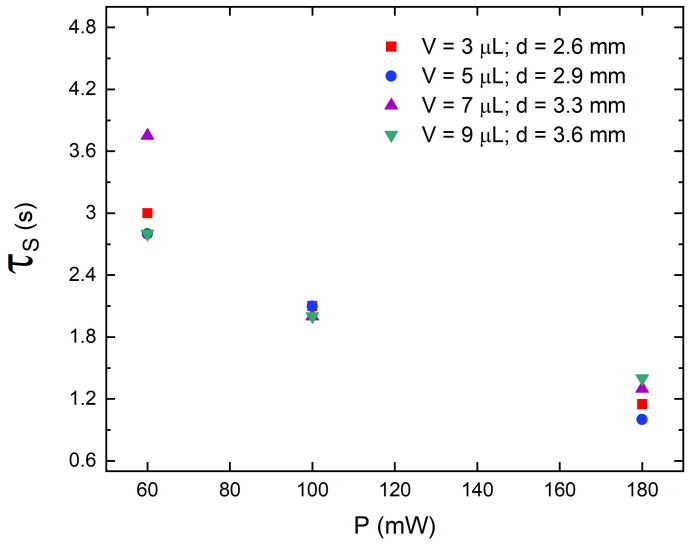

Figure 4.10: Second example plot of how the stopping time (τ_S) changes as a function of the illumination power (P). The droplet volume changes, while the spot diameter remains the same and equal to 1.1 mm.

4.3 Droplet movement along a path

After having characterized the attraction phenomenon, the next step of the experimental measurements has the main goal to trying to move a water droplet along a specific path. The basic idea regarding the movement of the fluid is exploiting again the interaction between the neutral droplet and the electric field created due to the illumination of Lithium Niobate sample, where the droplet is attracted towards the illuminated area; but in order to make the droplet following a specific path in the space it's necessary to illuminate different spatial regions of the sample in sequence in time.
This specific illumination process is obtained using the Slide-Show software, which can control the SLM device: first it's important to choose the shape and dimensions of the illumination pattern. Then a sequence of images showing the shape of illumination pattern moved in space between one image and the subsequent one needs to be created. Finally, giving in input the previous sequence of images, the SLM allows to create the desired path, by projecting and illuminating different regions of the Lithium Niobate in sequence in space and time (in the sense that passing from one illuminated area to the subsequent one, the illumination of the previous region is switched off). Furthermore this SLM software allows to choose manually the time instant at which it's possible to change the illumination of different regions of the path in order to have a better control of the droplet motion along the path.
Another major requirement concerns the realization of the path along which the droplet should move: one illuminated region and the following one needs to be a little bit superimposed in space. In fact if there is no superposition, the droplet could follow just one or two parts of the path and after that or it's repelled out or it does not feel the attraction towards the following illuminated area anymore without moving from it's position. Moreover the superposition between 2 following illuminated regions doesn't need to be excessive, otherwise in the common area too much charges accumulate so that it becomes very difficult to control the droplet motion, driving it on the desired spatial path because the droplet is repelled out very quickly.
Furthermore the Lithium Niobate sample is not illuminated by setting the maximum available value for the laser power reaching the sample (180 mW), but choosing power values between 80

mW and 120 mW otherwise it would become very difficult to drive the droplet along the chosen path due to repulsion effects.
The volume of the moving droplets is 3 μL or 5 μL, otherwise droplets with a greater volume are not able to follow the entire chosen path because at one point they stop at a specific position of the path and it becomes practically impossible to put these droplets in motion again.
Regarding the path that the droplets should follow, it will be constituted by a sequence of circular spots, illuminated at different time instant according to the spatial position of the droplet along the chosen path. Considering the attraction measurements performed in the previous sections, in principle the spot diameter could vary between 3 mm, 1.1 mm, 0.8 mm or 0.5 mm, that are really the values chosen for the size of the illumination pattern to collect the previous data. But preliminary tests display that the droplet was able to follow only one or two parts of a path formed by circular spots with diameters of 0.8 mm or 0.5 mm because the droplet was repelled away easily and very quickly. While in preliminary measurements performed constituting a path with spots with diameter equal to 3 mm or 1.1 mm, the droplet was able to follow the entire or almost entire the path chosen and the repulsion process was easier to control and avoid with respect to the other 2 cases. For these reasons in all the following measurements the droplet manipulation will be obtained considering paths constituted by spots with diameters of 3 mm or 1.1 mm.
These measurements are performed choosing 2 different paths a linear one and a curved one in order to show that a water droplet can be driven along any kind of path of choice.

4.3.1 Motion on a linear path

The first kind of motion is obtained by driving a water droplet along a linear path from right to left. As example in Fig. 4.11 there is a sequence of frames, showing both the moving droplet and the illuminated areas, constituting the linear path followed by the droplet. The water droplet has a volume of 3 μL and the linear path is created by a sequence of circular spots with diameter of 3 mm. The illumination of the areas is continuous in time and homogeneous in space and the power of the laser reaching the sample is 100 mW. The video acquisition is obtained thanks to the camera, that allows to have a lateral view of the phenomenon. In the first frame of the sequence the red arrow indicates the direction of motion of the droplet along the path.

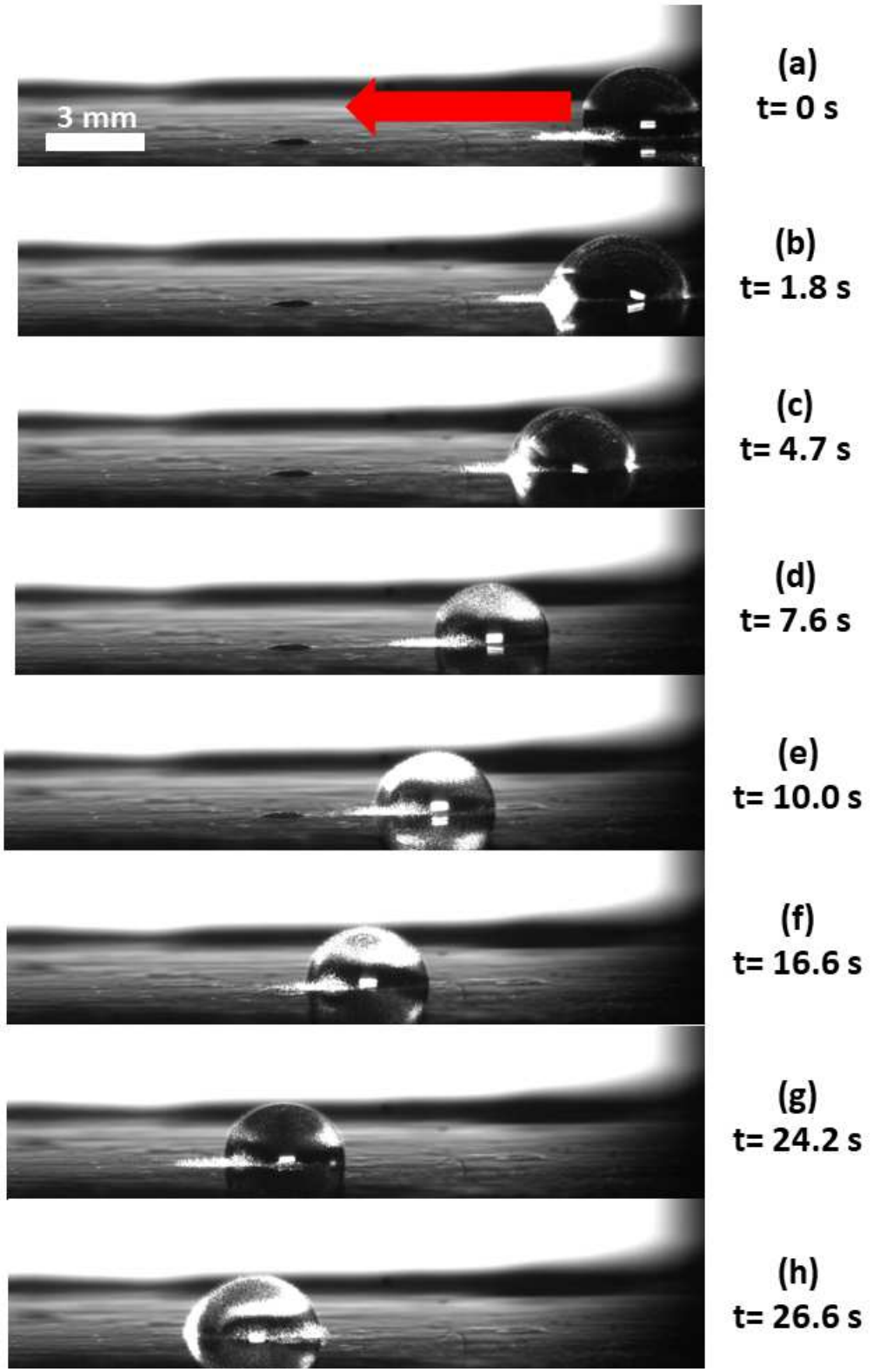

Figure 4.11: Sequence of frames showing the movement of a water droplet along a linear path.

4.3.2 Motion on a curved path

The second kind of motion occurs along a curved path with a shape, resembling the letter "S". As in the previous example of motion along a linear path, the illumination of different region of the sample in time and space is obtained by exploiting the Slide-Show software controlling the SLM, after that the right sequence of images has been created and then put in input in the Spatial-light modulator itself. In Fig. 4.12 a sequence of frames is presented so that it's possible to show the motion of the droplets along the chosen curved path. In this example the volume of the water droplet is 3 μL and the curved path is created by illuminating different regions of the sample with a sequence of circular spots with 3 mm as diameter. The different areas are illuminated in a continuous and homogeneous way and the power of the laser reaching the sample is 100 mW. The video acquisition is obtained thanks to the Basler camera equipped with the Navitar objective, allowing a vision of the sample from bottom (the other camera for the lateral view doesn't allow to display the motion along a curved path). During the acquisition it's necessary to mount a green filter between the dichroic mirror and the objective of the camera otherwise a green light would have pervaded the entire field of view of the camera, making impossible to observe the motion of the droplet.
In the frames from (a) to (k) of the frame sequence in Fig. 4.12 the full green circles indicates the specific circular illumination pattern used to put in motion the water droplet at a specific time instant; instead the dotted and empty green circles show the sequence of regions previously illuminated at different time instants and in different spatial positions, that allows to reconstruct the trajectory followed by the droplet during its motion. In the last frame (i) the entire spot sequence is shown and some green arrows display the entire curved path covered by the droplet (moreover in frame (i) the initial and the final position of the droplet along the curved path are shown).

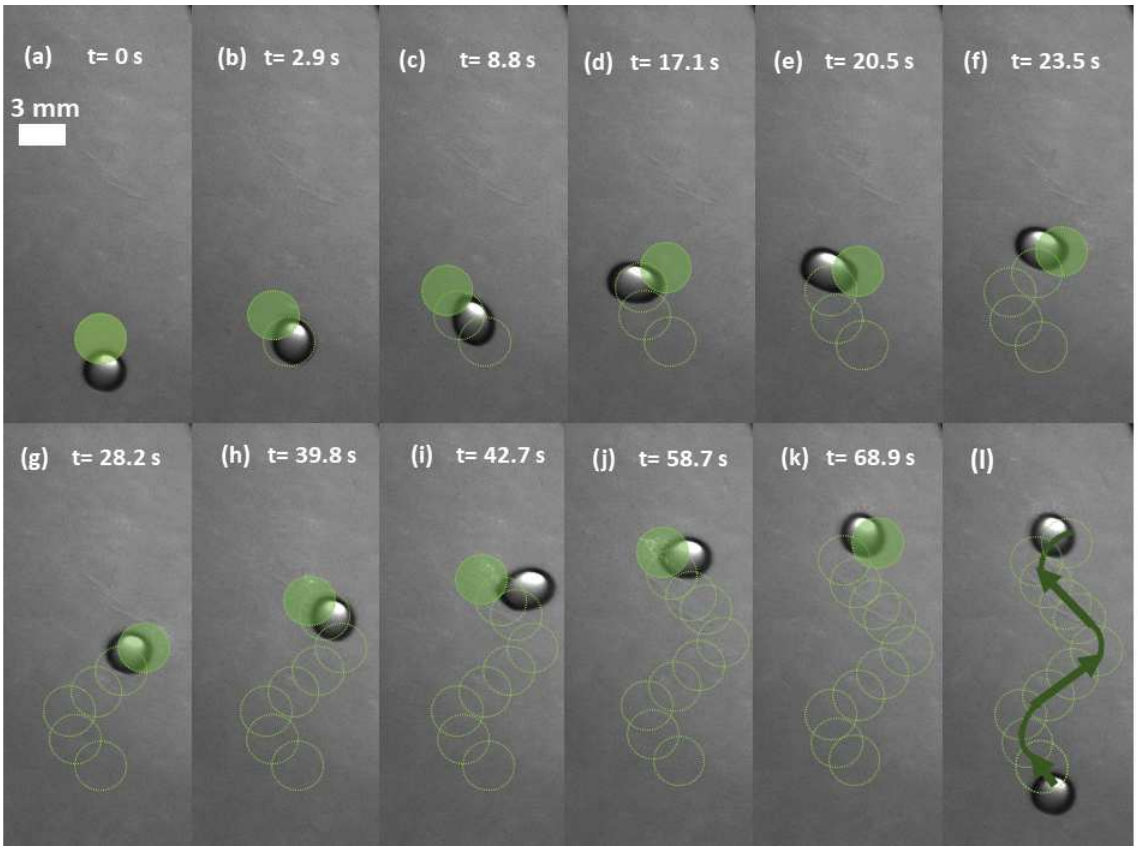

Figure 4.12: Sequence of frames, showing the motion of a water droplet along a curved path.

4.4 Merging of droplets

The next part of the measurements has the main goal to move one or more droplets and obtaining finally the merging between the different moving bodies. The motion of one or more droplets exploits again the interaction between the neutral droplet and the electric field generated due to LN sample illumination; the main difficulty of this process consists in driving along the desired paths and controlling the motion of different droplets simultaneously.
As in the case of driving one single droplet, the paths, that the droplets should follow, are constituted by illuminating different spatial areas of Lithium Niobate sample at different time instants. The practical realization is obtained by exploiting again the Slide-Show software, which allows to control the spatial light modulator after having created the right sequences of images forming the desired paths.
The merging process is studied by realizing 3 measurements with an increasing number of degree of freedoms and of difficulties consequently:

- merging between one moving droplet and one steady droplet;
- merging of two moving droplets simultaneously in two counter-propagating directions;
- merging of three moving droplets simultaneously.

4.4.1 Merging case 1: one moving droplet and one steady droplet

In the first case (the "easiest" one to be realized) an example of the merging process between one moving droplet and one steady droplet is shown in the sequence of frames in Fig. 4.13 (in frame (a) the red arrow indicates the direction of motion of the moving droplet). The moving water droplet is forced to follow a linear path from right to left, connecting it to the other droplet; the path is constituted by illuminating different areas of the sample creating a sequence of circular spots of 3 mm as diameter spaced in space and time properly; the illumination of one specific area is continuous in time and homogeneous in space. In the shown example the volume of the 2 droplets is the same and equal to 3 μL and the illumination power set reaching the sample is 100 mW. Since the motion occurs along a straight line, the video recording is obtained by exploiting the camera for the lateral view of the phenomenon.

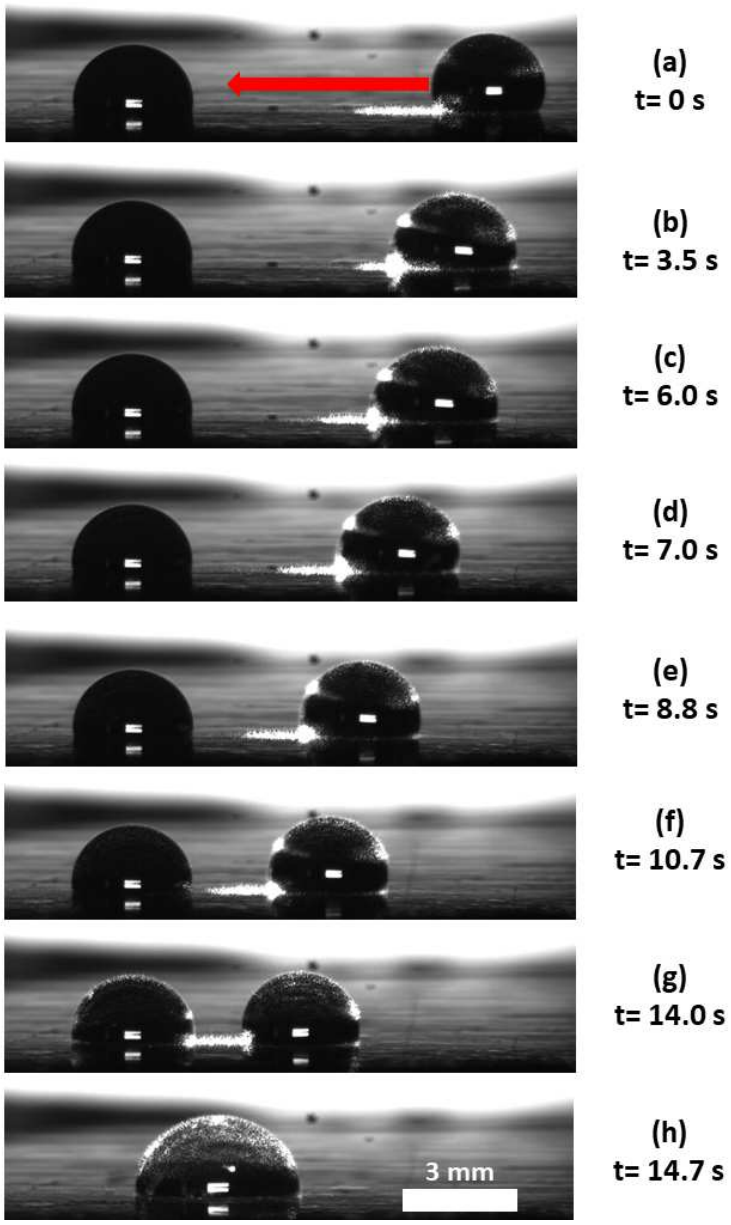

Figure 4.13: Sequence of frames, showing the merging between one moving droplet from right to left and a steady droplet

4.4.2 Merging case 2: two moving droplets in two opposite directions

The second case deals with the merging process between two water droplets moving in two counter-propagating directions along a linear path; a sequence of frames of an example measurements is shown in Fig. 4.14 (in frame (a) the two red arrows indicate the motion directions of the 2 droplets). As described in the previous paragraph, the main difficulty of this kind of process rises because the two droplets needs to move simultaneously and should follow in principle the same linear path in two opposite directions. The desired linear path is constituted by giving in input in the SLM a sequence of images, in which two areas of the Lithium Niobate sample symmetric with respect to the centre of the entire linear path are illuminated and between one image and the subsequent one the two illuminated symmetric zones become closer to the centre of the linear path. In the following example the illumination path is constituted by a sequence of circular spots with 3 mm as diameter and the power of the laser reaching the sample is 100 mW; the illumination of different areas is continuous in time and homogeneous in space. The volume of the two moving droplets is the same and equal to 3 μL and the video recording is again obtained using the camera for the lateral view of the sample.

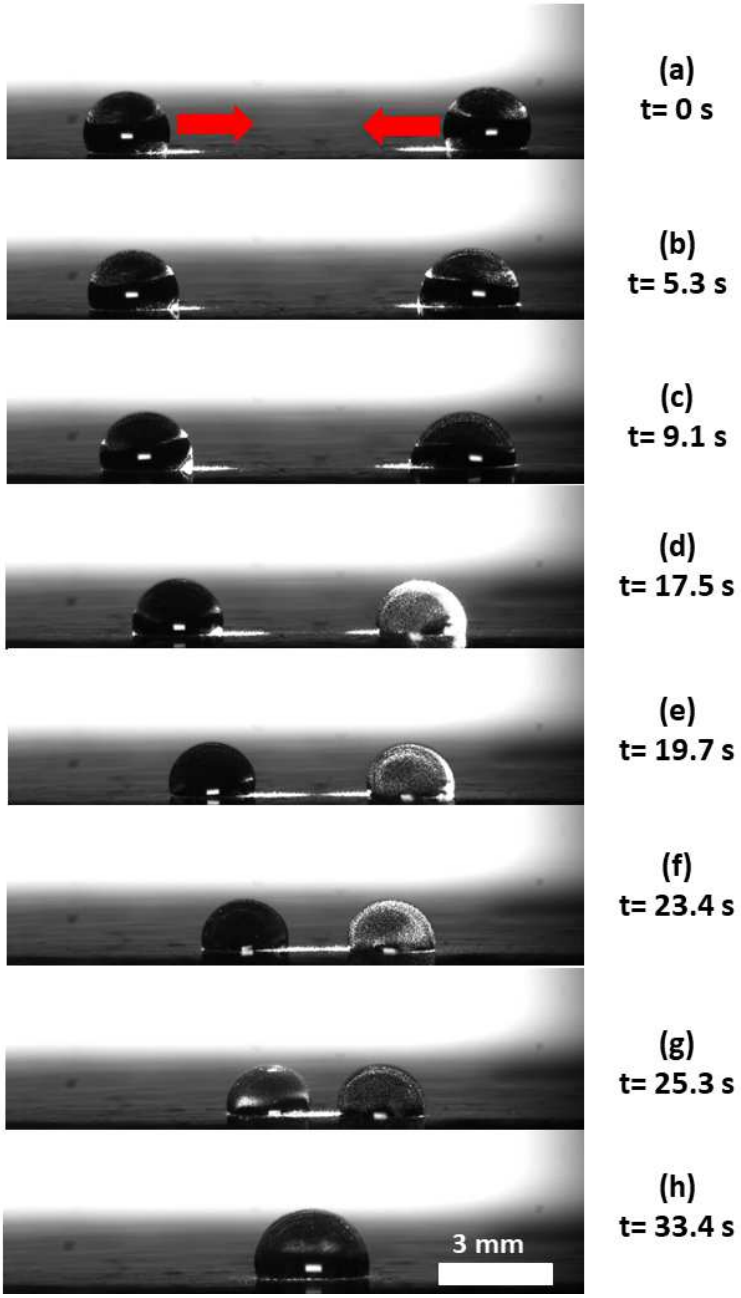

Figure 4.14: Sequence of frames, showing the merging process between two droplets moving in two counter-propagating directions.

4.4.3 Merging case 3: merging of 3 moving droplets

The last case for these measurements (the most difficult one) deals with the merging process of three moving droplets simultaneously, whose one example is shown in Fig. 4.15 thanks to a sequence of frame images of the process. In this situation the difficulties become greater with respect to the previous cases since the three droplets should move together and at the same time following three different linear paths till the merging in one greater droplet.
The paths followed by the droplets are constituted by giving in input in the SLM a sequence of images in which the illuminated areas of the sample should form the vertices of an approximate equilateral triangle; between one image and the subsequent one the illuminated areas move in space exploiting the Slide-Show software of the spatial-light modulator, approaching approximately the centre of the triangle more and more As a consequence each single droplet is forced to following a linear path from its initial position till the centre of the equilateral triangle approximately.
In the example in Fig. 4.15 the illumination paths are constituted by a sequence of circular spots with 3 mm as diameter; the illumination of the areas is again continuous in time and homogeneous in space with a power of 100 mW at the position of the sample. The volume of the three moving droplets is equal to 3 μL for each one and since the motion doesn't occur just only a straight line, the video recording is obtained thanks to the camera equipped with the Navitar objective, that allows to observe the sample from bottom. In the frames from (a) to (h) the green full circles indicate the position of the illuminated areas with respect to the three moving droplets at different time instants.

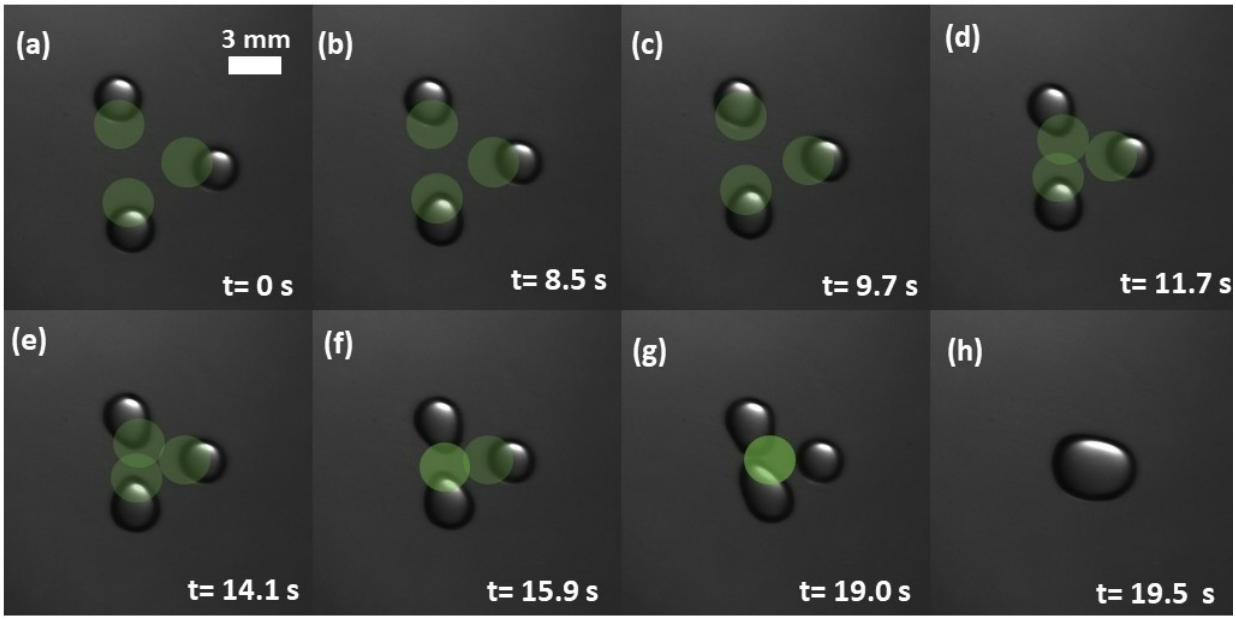

Figure 4.15: Sequence of frames, showing the merging process between three moving droplets.

4.5 Repulsion of a droplet

The repulsion of the water droplet usually occurs after an attraction event whether the droplet has been attracted and put in motion towards the illuminated area or whether the droplet only feels an attraction, but it doesn't move from its initial position. Moreover this process happens for all the droplet volumes considered (3 μL, 5 μL, 7 μL and 9 μL) and almost all the laser powers values used to illuminate the Lithium Niobate sample (from 60 mW to 180 mW); but the instant of time for which the droplet is repelled far away from the illumination pattern changes drastically. Moreover the direction on which one droplet is repelled far away from the illuminated area isn't so easy to be controlled. In fact it could happen that between two measurements performed with exactly the same parameters (laser power, illumination pattern, droplet volume and mutual position between droplet and illuminated area) the droplet is repelled in two completely different directions.
Since controlling the dynamics of the repulsion process is very difficult, in this thesis work the repulsion phenomenon of a water droplet has not been studied in details and systematically. Maybe a thesis project should be totally devoted to the study of repulsion in order to characterize properly the phenomenon computing the repulsion time and understanding better the direction in which the droplet is repelled out by tuning different experimental parameters such as the shape, dimensions and power of the illumination pattern or the mutual position between the droplet and the illuminated area itself or the volume of the droplet itself.

4.6 Splitting of a droplet

The next measurements are devoted to trying to study the splitting event of a water droplet. It's noteworthy to recall that in literature in scientific papers dealing with Lithium Niobate samples, the splitting a water droplet is in general obtained by exploiting the properties of a y-cut Lithium Niobate sample [34]; instead in the case of a z-cut Lithium Niobate (the kind of sample used for the measurements described in this thesis work) it's more difficult and challenging to split a water droplet in two or more parts. The difference is related to the fact that in a y-cut sample the electric field lines are parallel to the face of the illuminated sample and this configuration helps a lot when the splitting event needs to occur. Instead in the z-cut sample the electric field lines are orthogonal to the illuminated face of the sample, making the splitting of the droplet more difficult to happen. In Fig. 4.16, a visual scheme of a z-cut and y-cut sample is shown and in particular the field lines are highlighted thanks to white arrows (in both cases the $LiNbO_3$ sample is illuminated from bottom).
Different measurements have been performed in order to obtain the splitting of a water droplet exploiting different illumination patterns such as circular spots or linear and curved stripes; but in most of the cases the splitting event doesn't occur. Moreover when it was able to split the droplet with a specific illumination pattern, in the subsequent measurements performed in the exact same experimental conditions (droplet volume, shape and size of the illumination pattern and illumination power) the splitting event doesn't occur instead, confirming the difficulties in reproducing this physical phenomenon using a z-cut Lithium Niobate sample experimentally.
During the measurements accidentally the splitting of water droplet was in two different configurations:

- when it was trying to obtain the merging process of three water droplets moving simultaneously, in some cases one water droplet stops to follow the linear path constituted by a sequence of spots and suddenly splits in two parts, one remaining over the the illuminated area and the second one was repelled in another direction.

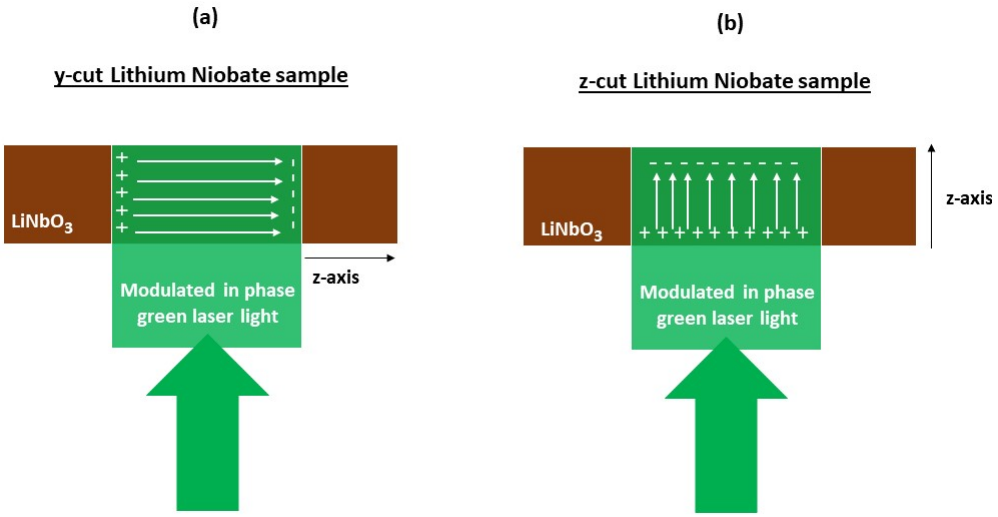

Figure 4.16: Example of y-cut (on the left) and z-cut (on the right) Lithium Niobate samples with the field lines in evidence. The green arrows indicates that laser light comes from bottom for illumination.

- when it was studying the motion of a droplet along a stripe with a linear gradient of illumination in one case the droplet starts to move following the linear path, but at a certain point along the stripe it stopped and split in two parts, one remaining again over the stripe and one was repelled in another direction.

When it was trying to obtain the splitting event in a controlled and not accidental way, it was decided to operate in a way similar to the one described in some scientific papers: in these one the splitting event is obtained by illuminating with the maximum possible power reaching the Lithium Niobate sample a water droplet with a volume smaller than 1 μL thanks to a linear stripe with dimensions greater than the typical size of the droplet itself. For these kind of measurements it was decided to create a linear stripe with dimensions of 4 mm in width and 12 mm in length and illuminated in a homogeneous and continuous way with a power of 180 mW; the droplet needed to be split had a volume of 0.8 μL and it was put at the center of the stripe approximately. In Fig. 4.17 the water droplet before (on the left) and after (on the right) the splitting event is shown and moreover in evidence there is the stripe exploited to achieve the desired goal; that's one of the only two cases in which it was possible to obtain a splitting event in a controlled way.
In Fig. 4.17 it's possible to notice that the water droplet splits into 3 parts: one very small and almost imperceptible portion remaining over the stripe; one portion moving in the left horizontal direction approximately and the third part instead moves horizontally right and towards the bottom part of the stripe. It's important to claim that there is only a preliminary study of the splitting event of a water droplet; a more systematic study will require: first achieving the splitting event in a more reproducible way from an experimental point of view. Moreover the splitting process should be studied by changing different experimental parameters: the droplet volume, the shape and size of the illumination pattern and the illumination power.

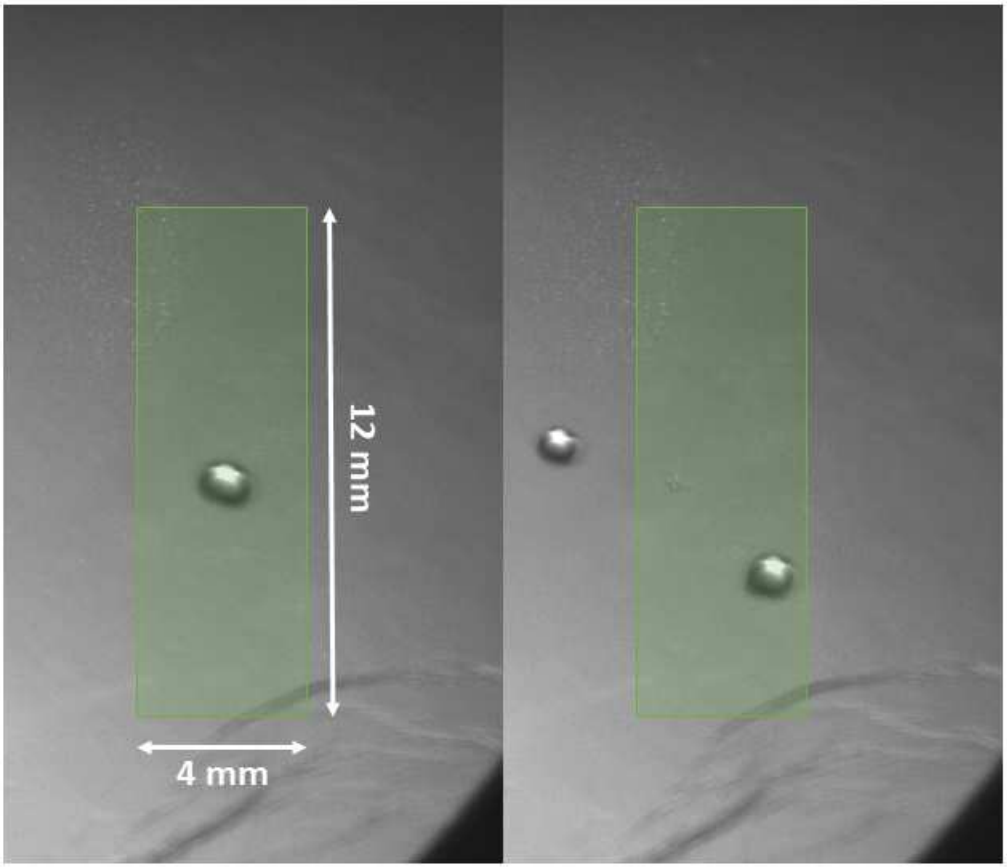

Figure 4.17: Example of splitting of a water droplet: on the left the droplet before splitting; on the right the droplet after the splitting event.

4.7 Motion over a stripe non-homogeneously illuminated

As last measurements it's studied the motion of a water droplet along a stripe non-homogeneously illuminated: this particular illumination pattern is created by giving in input in the SLM device an image with a linear gradient in the grey-scale ranging from 0 to 255.
Two different configurations are exploited: the first one using a stripe with 5 mm as width and 15 mm as length and the second one using a stripe with 5 mm and 7.5 mm as length. The droplet starts its motion from the region of the stripe, where in the input image there are the lowest values of the grey-scale; then it's expected that the water droplet starts to feel the attraction and moves following the gradient in the illumination pattern and finally, after having reached the final part of the stripe (the most illuminated one), the droplet should be repelled along the direction followed by the linear stripe.
In the 2 following figures (Fig. 4.18 and Fig. 4.19) different sequences of frames are created in order to show the motion along the 2 different in length linear stripes. In both cases a 3μL droplet is put in motion, the illumination power set is 180 mW (the maximum possible value) and the video acquisition is obtained with the camera for lateral view, that allows to appreciate the gradient in illumination in a good way. In both examples in the first image there is shown

the stripe with the gradient in illumination and its characteristic dimensions, that will be given as input image in the SLM in order to create the desired pattern. In both examples the second image (a) is characterized by the presence of a red arrow, indicating the direction of motion of the droplet itself.

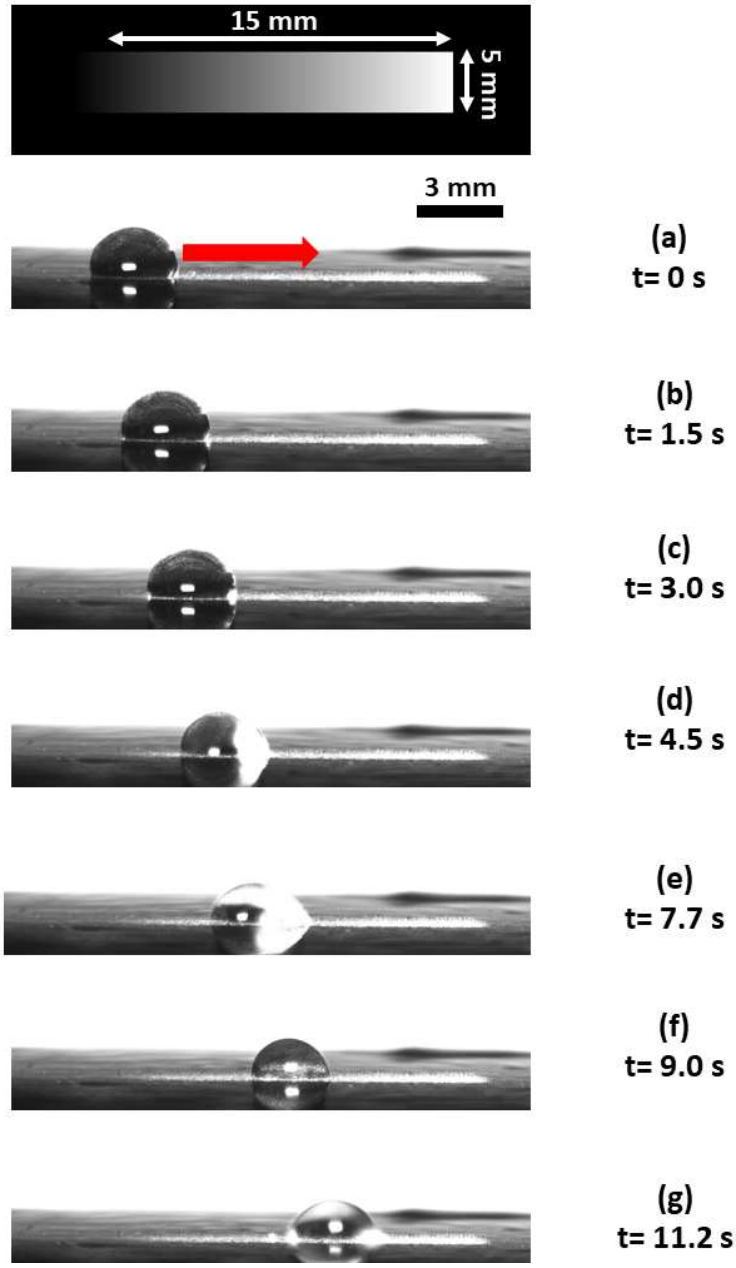

Figure 4.18: Motion of a droplet along the longer stripe with a linear gradient of illumination.

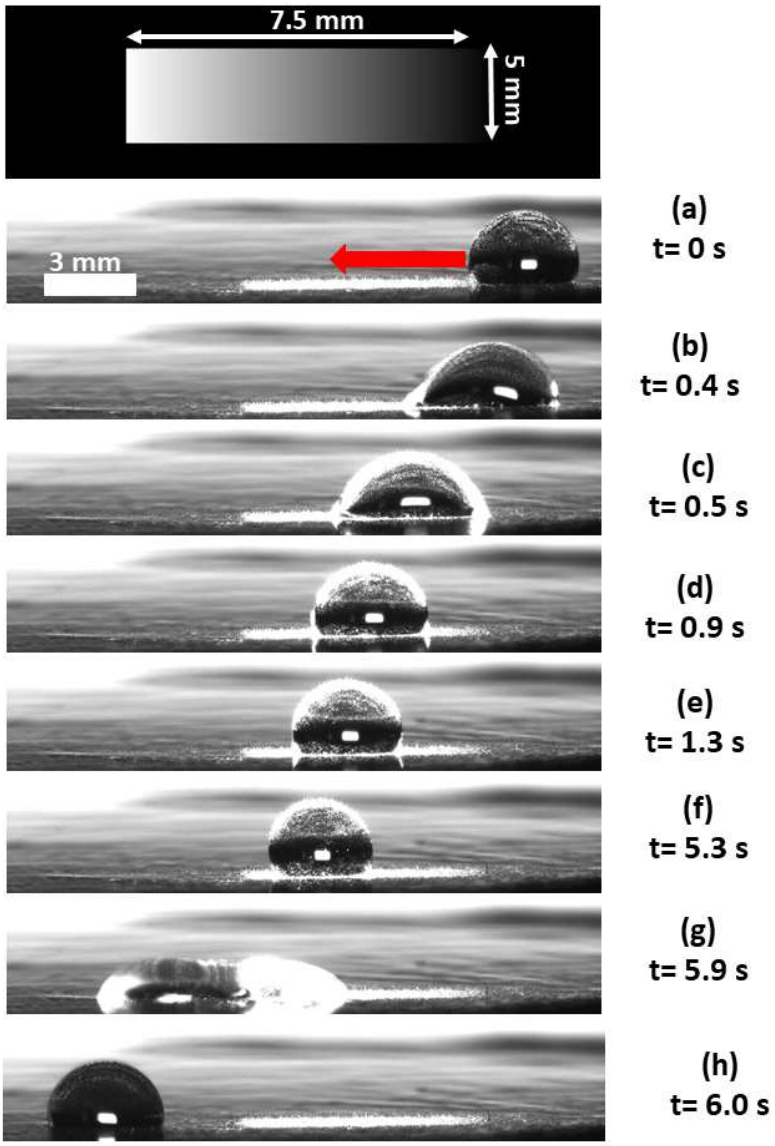

Figure 4.19: Motion of a droplet along the shorter stripe with a linear gradient of illumination.

Observing the 2 different sequences of frames (Fig. 4.18 and Fig. 4.19), it occurs what expected: the droplet feels the attraction towards the illumination pattern and then it moves following the gradient in illumination of the pattern itself. In the case of the shorter stripe (Fig. 4.19) the droplet is able to reach the end of the stripe and then it's repelled away along the direction corresponding to the gradient in illumination; instead in the case of the longer stripe (Fig. 4.18) the droplet reaches a specific point along the stripe and then it's repelled in the direction orthogonal to the one corresponding to the gradient in illumination.
As in the case of the splitting, these are only preliminary measurements showing that a water droplet can follow a pattern non-homogeneously illuminated in space, but characterized by a linear gradient in illumination. A more systematic study of this phenomenon can be performed by tuning some experimental parameters such as: the droplet volume, the characteristic dimensions of the stripe or the illumination gradient of the pattern. This study would be important to understand in which condition the droplet is able to follow the path entirely or in some parts, when it's repelled away and what parameters affect this specific behaviour.

4.8 Discussion of the experimental results

The role of humidity on $LiNbO_3$ discharge is studied in a qualitative way, exploiting an indirect measurement (pendant drop measurements) since the electric field related to the photovoltaic effect of LN cannot be measured directly. In the pendant drop measurements it should be noticed that the falling distance of a water droplet decreases while the humidity value around LN sample increases and this qualitative trend is discovered in 3 different configurations, where the waiting time is changed ranging from 30 seconds till 20 minutes. This behaviour shows humidity is able to affect the charge accumulation and accelerate the $LiNbO_3$ discharge. The next step would be making more systematic measurements to obtain direct information on the electric field related to the photovoltaic effect and its time evolution.
The second part of the experimental measurements was aimed to control the movement of water droplet on LN sample. The basic physic phenomenon related to droplet manipulation is the dielectrophoretic force due to the interaction between the electric field and the neutral water droplet. The attraction process towards the illuminated area was studied by tuning different experimental parameters such as droplet volume and the illumination; the response time for attraction and then the stopping time, moving the droplet towards the illuminated area, modifying the size of the illumination pattern in this case, have been extensively investigated.
After that the attention was focused to move a water droplet on a chosen path: two different geometries were realized starting from a simple linear path to a more complex curved path. In both the examples the droplet was able to follow entirely the chosen paths.
Given the motion of one single droplet, the next natural step was to realize a merging process by considering the merging between one moving and one steady droplet, the merging between two moving droplets in two opposite directions and the merging between three moving droplets simultaneously.
Finally preliminary observations of the splitting process and the motion over a stripe with non-homogeneous illumination were reported. In the future, the next measurements should be devoted to characterize the repulsion effect, that has not been studied in this work because both the repulsion time and direction were not well controlled.

Conclusions

This master thesis considered two main aspects of optowetting on LN: (i) the role of humidity on Lithium Niobate discharge, when the illumination is switched off and (ii) the control of the motion of water droplets exploiting the photovoltaic properties characterizing Lithium Niobate itself. In the following the major outcomes of this work are recap by recalling the most representative results showed in chapter 4.

(i) Role of the humidity on $LINbO_3$ discharge

Regarding humidity, it is noteworthy to recall that, to the best of our knowledge, there are no scientific articles in literature addressing the role of humidity on Lithium Niobate discharge; as a consequence this part of the thesis activity could be considered a sort of pioneering work in understanding the relation between the photovoltaic properties of LN and the environmental conditions (humidity in this case) in which the experimental data are collected. The measurements realized (subsection 4.1.2) display that by increasing the humidity value considered from 30% to 80% (the usual working range) the falling distance gradually decreases. This indicates that Lithium Niobate is not only characterized by an intrinsic discharge, but also the environmental conditions, in particular humidity, in which the measurements are performed, can affect the charge accumulation over the surface of Lithium Niobate itself (an example plot in Fig. 4.20).

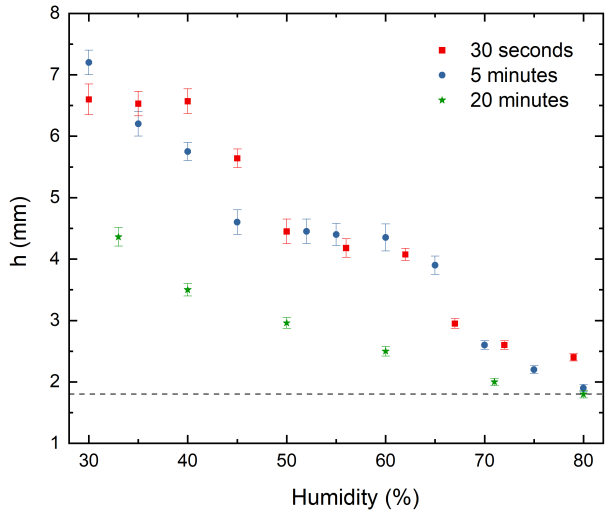

Figure 4.20: Falling distance (h) values as a function of humidity around $LINbO_3$ sample.

(ii) Droplet motion

Regarding droplet manipulation, as first step the attraction phenomenon is studied: by illuminating a certain region of the Lithium Niobate sample with a circular spot, a water droplet is attracted towards the illuminated region due to the dielectrophoretic effect. In this configuration both the response time and the stopping time have been studied by varying the illumination power, the volume of the droplets and in the case of the stopping time measurements the illumination spot diameter was also modified. One of the most relevant results is that the response time for attraction does not depend on the droplet volume and it displays a saturation effect for illumination power higher than 100 mW. Conversely the stopping time shows a similar behaviour when the spot size dimension is fixed. Moreover the stopping time is rather independent from the illumination pattern size.
After that the droplet was put in motion along selected paths: one path was simply linear and the second one was a curved path resembling a "S" letter (see Fig. 4.21 for the motion along a linear path).
After that since it was possible to put in motion one single water droplet along a desired path, the merging process was studied: in particular three different configurations were studied.

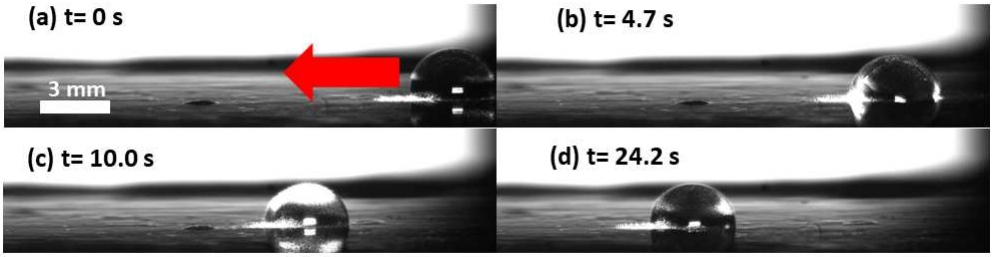

Figure 4.21: Sequence of frames for the motion along a linear path.

(iii) Preliminary results and future measurements

Finally preliminary measurements were performed in order to obtain the splitting of a water droplet and to study the motion of a droplet along a linear stripe with a linear gradient in illumination (in Fig. 4.22 an example of the input image sent in the SLM, showing a stripe with linear gradient exploited to study the droplet motion over a stripe non-homogeneously illuminated).

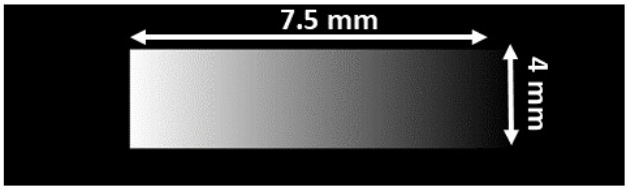

Figure 4.22: Input image of the SLM, showing a stripe with a linear gradient in illumination.

In the next future more systematic studies should be performed in order to extrapolate quantitative information from the droplet motion along a certain path or the merging process, trying to

compute the velocity of the moving droplets. Moreover an accurate study should be realized in order to characterize the repulsion phenomenon, computing typical times and trying to understand the influence of experimental parameters on the direction in which the droplet is repelled away from the illumination pattern. A similar study would be required in trying to understand the motion of a droplet along a stripe with a gradient in illumination. Finally the splitting process should need to be obtained in a more reproducible way, overcoming the limitations of the z-cut Lithium Niobate sample, by exploiting different illumination configurations and tuning the droplet volume.

Bibliography

[1] George M. Whitesides. The origins and the future of microfluidics. *NATURE*, 442(7101):368–373, JUL 27 2006.

[2] Chen S. and Tabeling P. Introduction to microfluidics. *OUP Oxford*, 2005.

[3] Hughes P. Eliminating sticky situations with Adaptive Surface Technologies. *Chemistry World*, 2020.

[4] G. Mistura and M. Pierno. Drop mobility on chemically heterogeneous and lubrificant-impregnated surfaces. *Advances in Physics:X*, 2(3):591–607, 2017.

[5] Bohn H. F. and Federle W. Insect aquaplaning: Nepenthes pitcher plants capture prey with the peristome, afully wettable water-lubrificated. *Proceedings of the National Academy of Sciences*, 101(39):14138–14143, 2004.

[6] Varanasi K. K. et al. Droplet mobility on lubrificant impregnated surfaces. *Soft Matter*, 9(6):1772–1780, 2013.

[7] Mugele F. and Baret J.C. Electrowetting: from basics to applications. *Journal of Physics: condensed matter*, 17(28), 2005.

[8] Weis R. and Gaylord T. Lithium Niobate: Summary of Physical properties and crystal structure. *Applied Physics A*, 37(4), 1985.

[9] Carneri M. Control of drop motion by means of optical patterns imprinted on Fe:$LiNbO_3$ crystals. *Master degree thesis, University of Padua*, 2021.

[10] Caputo D. et al. Drop position sensing in digital microfluidics based on capacitance measurement. *Conference: 2015 XVIII AISEM Annual Conference*, 2015.

[11] De Gennes P. G. et al. Capillarity and wetting phenomena: drops, bubbles, pearls, waves. *Springer Science and Business Media*, 2013.

[12] Zhao H. and Law K. Y. Surface wetting: characterization, contact angle and fundamentals. *Springer Switzerland*, 2016.

[13] Ras R. H. et al. Surface-wetting characterization using contact-angle measurements. *Nature protocols*, 13, 2018.

[14] Gillner A. et al. Influence of self-organizing microstructures on the wettability of molten plastic on steel for hybrid plastic-metal joints. *Welding in the world*, 63, 2019.

[15] McCarthy T. J. and Gao L. Contact angle hysteresis explanation. *Langmuir*, 22(14), 2006.

[16] Nishimoto S. and Bhushan B. Bioinspired self-cleaning surfaces with superhydrophobicity, superoleophicity and superhydrophilicity. *RSC Advances*, 2013.

[17] Kang S.H. et al. Bioinspired self-repairing slippery surfaces with pressure stable omniphobicity. *Nature*, 477, 2011.

[18] Hardt S. et al. Simple fabrication of water-repellent surfaces with low contact-angle hysteresis based on impregnation. *Advanced Materials Interfaces*, 1(1), 2014.

[19] Varanasi K. K. et al. Enhanced condensation on lubrificant-impregnated nanostructured surfaces. *ACS nano*, 6(11), 2014.

[20] Quere D. et al. Universality of friction laws on liquid-infused materials. *Physical Review Fluids*, 5, 2020.

[21] Lee Y. et al. Lubrificant-infused directly engraved nano-microstructured for mechanically durable endoscope lenses with anti-biofouling and anti-fogging properties. *Nature*, 2020.

[22] Latthe S. S. et al. Recent developments in air-trapped superhydrophobic and liquid-infused slippery surfaces for anti-icing applications. *Elsevier*, 2019.

[23] Berge B. Electrocapillarité et mouillage de films isolant par l'eau. *Comptes rendus de l'Academie des sciences, Serie 2, Mecanique, Physique, CVhimie, Science de l'univers, sciences de la Terre*, 317, 1993.

[24] Umar A. et al. Bifunction-Integrated Dielectric Nanolayers of Fluoropolymers with Electrowetting Effects. *Materials*, 11(12), 2018.

[25] Liu Y. et al. Electtowetting on liquid-infused film (ewolf): complete reversibility and controlled droplet oscillation suppression for fast optical imaging. *Scientific Reports*, 2014.

[26] Volk T. and Wohlecke M. Lithium Niobate: defects, photorefraction and ferroelectric switching. *Springer Science and Business Media*, 115, 2008.

[27] Sclarb U. and Beltzer K. Refractive indices of Lithium Niobate as a function of wavelength and composition . *Journal of Applied Physics*, 73(7), 1993.

[28] Grilli S. and Ferraro P. Dielectrophoretic trapping of suspended particles by selective pyroelectric effect in Lithium Niobate crystals . *Applied Physics Letters*, 92(23), 2008.

[29] Glass A. et al. High-voltage bulk photovoltaic effect and the photorefractive process in $LiNbO_3$. *Landmark papers*, 1995.

[30] Buse K. et al. Photorefractive properties of highly-doped Lithium Niobate crystals in the visible and near-infrared . *Applied Physics B*, 68(5), 1999.

[31] Carrascosa M. et al. Time evolution of photovoltaic fields generated by arbitrary light patterns in z-cut $LiNbO_3$:Fe: application to optoelectronic nanoparticle manipulation. *Optics Express*, 36(9), 2020.

[32] Kukhtarev N.V. Kinetics of hologram recording and erasure in electro-optic crystals. *Pisma Zhurnal Tekhnischeskoi Fiziki*, 1976.

[33] Carrascosa M. et al. Real-time operation of photovoltaic optoelectronics tweezers: new strategies for massive nano-object manipulation and reconfigurable patterning. *Particle Systems Characterization*, 36(9), 2019.

[34] Puerto A. et al. Optoelectronic manipulation, trapping, splitting and merging of water droplets and aqueous biodroplets based on bulk photovoltaic effect. *Physical Review Apllied*, 14(2), 2020.

[35] Brinker C. J. Dip coating. *Springer*, 2013.

[36] Meggiolaro A. Motion control of water droplets by means of optical pattterns imprinted on Fe:$LiNbO_3$ crystals. *Master degree thesis, University of Padua*, 2020.